

Lawrence Berkeley National Laboratory

Recent Work

Title

MSA Short Course: Molecular Geomicrobiology Molecular-Scale Processes Involving Nanoparticulate Minerals in Biogeochemical Systems

Permalink

<https://escholarship.org/uc/item/2fj1z04t>

Journal

Molecular Geomicrobiology, 59

Author

Banfield, Jillian F.

Publication Date

2005

MSA Short Course: Molecular Geomicrobiology

Molecular-Scale Processes Involving Nanoparticulate Minerals in Biogeochemical Systems

Benjamin Gilbert

Earth Sciences Division

Lawrence Berkeley National Laboratory

Jillian F. Banfield

Earth & Planetary Sciences

UC-Berkeley

INTRODUCTION

Mineral particles with diameters on the scale of nanometers (nanoparticles) are important constituents of natural environments. The small size of such particles has a host of consequences for biogeochemical systems, which we will review in this chapter. We begin by briefly reviewing what is known about how and when nanoparticles form and the ways in which nanoparticles impact natural processes.

Nanoparticles form via a variety of inorganic and biological pathways and may be introduced into the environment as a consequence of human activity. They are widespread in the environment (Penn et al. 2001, Banfield & Navrotsky 2001, van der Zee et al. 2003, Kennedy et al. 2003a, 2003b), although few quantitative studies of their abundance are available. While all crystals begin as very small particles, an important subset retain small size at the Earth's surface over relatively long time scales, because the combination of low temperature and low solubility inhibits growth. As a consequence,

nanoparticles have the potential for a long lifetime in the environment, and widespread transport under certain circumstances.

Processes that result in the removal of nanoparticles from an environment include dissolution, settling from air, transport in solution, and crystal growth. Particle aggregation may be an important component of these processes because it will promote settling, limit dispersal via solution transport, and can lead to aggregation-based crystal growth.

The presence of nanoparticles can profoundly influence biological systems. Because they are frequently formed in environments that are populated by microorganisms, nanoparticles often adhere to cell surfaces or cell-associated polymers (see **Figure 1** for examples). These coatings can have important consequences for metabolic activity, for example, by restricting communication between the cell and its surroundings. They may also provide protection from predators, inhibit desiccation, screen cells from ultraviolet radiation, and alter the cell buoyancy (e.g., Tebo et al. 1997, Phoenix et al. 2001).

The controlled precipitation of nanoscale minerals can lead to formation of integrated organic-inorganic structures with diverse morphologies. In some cases, the shapes provide a record of past microbial activity (i.e., serve as biosignatures), possibly by preserving cell morphology, as seen in the iron oxyhydroxide nanoparticle coatings on extracellular sheaths of *Leptothrix*, **Figure 1**). Biominerals constructed from nanoparticles can be generated through deliberate action of the organism in order to create cell architecture (Mann 2000), and magnetic nanoparticles can serve a role in navigation (Bazylinski & Frankel 2004). However, in many cases the function is unclear or the particles may serve no function, and their existence is purely a byproduct of microbial metabolism (e.g., ZnS and UO₂ nanoparticles, **Figure 1**, and Mn(IV) oxides). Binding of nanoparticles to cell surfaces can also affect the fate and distribution of nanoparticles in the environment, by restricting or facilitating their transport, aggregation-based growth, and mineral transformation pathways. The interactions between nanoparticles, individual cells, and extracellular biomolecules can also act to bind biofilms together (Mayers & Beveridge 1989).

Sources of Nanoparticles in the Environment

A major pathway for nanoparticle formation in aqueous environments is the precipitation of sparingly soluble dissolved ions derived from both inorganic and biological processes. Precipitation is possible when the concentrations of ions in solution exceed the solubility of a mineral (e.g., see De Yoreo & Vekilov 2003). However, formation of a crystal nucleus is inhibited by an energy penalty associated with creation of a solid-liquid interface. Consequently, ion concentrations must generally exceed the saturation state of the solution for precipitation to occur. The relative energy cost associated with this interface is reduced as the particles grow, providing a driving force for coarsening.

Materials that form ultra-small particles are frequently very insoluble with low energy barriers for nucleation. Examples include UO_2 , with a solubility product for bulk material $\log K_{sp} \approx -60$, which forms 1–3 nm diameter particles (Suzuki et al. 2002, O'Loughlin et al. 2003); and ZnS, with a solubility product of $\log K_{sp} \approx -24$, which typically forms 2–3 nm diameter particles (Labrenz et al. 2001, Moreau et al. 2004). In fact, a wide range of both natural and synthetic nanoparticles initially forms in this size range.

Inorganic sources of environmental nanoparticles

A variety of inorganic pathways can lead to nanoparticle formation. Chemical weathering reactions that occur when minerals in rocks are exposed to water and air at the Earth's surface liberate ions that can reprecipitate as nanometer-scale silicate clay minerals, oxides, oxyhydroxides, and phosphates. Common examples include smectite (e.g., montmorillinite $(\text{Na,Ca})(\text{Al,Mg})_6(\text{Si}_4\text{O}_{10})_3(\text{OH})_6 \cdot n\text{H}_2\text{O}$), anatase (TiO_2), hematite ($\alpha\text{-Fe}_2\text{O}_3$), and rhabdophane ($\text{CePO}_4 \cdot \text{H}_2\text{O}$). Aqueous clusters of metal sulfides and aluminum oxide are found in some lake and marine environments (Rozan et al. 2000, Casey & Swaddle 2003). Nanoparticulate minerals may nucleate at sites on another mineral surface (Stack et al. 2004). Additional inorganic sources of nanoparticles include impacts, combustion, vaporization (e.g., breakdown of meteorites as they enter the atmosphere), evaporation of sea spray, erosion, faulting, and other mechanical processes.

Biological sources of environmental nanoparticles

Microbial activity is a major source of nanoparticles in the environment, and a summary of biogenic minerals is given in Frankel & Bazylinski, 2003. Central to microbial metabolism is the process of energy generation, which harnesses the free energy liberated as the result of coupled oxidation and reduction reactions. Reactions used for energy generation must be thermodynamically favorable, but are often kinetically inhibited. Organisms utilize enzymes to overcome these barriers and may speed up geochemical reactions by several orders of magnitude.

In many cases, minerals can serve as either reductant or oxidant in microbial metabolism. In the presence of reduced organic carbon, oxygen or nitrate often serve as the electron acceptor for microbial carbon respiration. However, electrons can be passed to ferric iron, Mn(III)/IV, or sulfate when oxygen and nitrate are not available (Edwards et al. 2000, Konhauser 1998, Banfield & Nealson 1997, Ehrlich 2002). Uranium ions can also be biologically reduced. In either metabolic or co-metabolic processes (Lovely et al. 1991, Abdelouas et al. 2000, Fredrickson et al. 2000), electrons are passed from organic carbon to aqueous uranyl (UO_2^{2+}) ions, resulting in the formation of insoluble uraninite (UO_2) nanoparticles.

Ferric iron and manganese minerals that act as electron acceptors are typically fine grained oxides that can dissolve upon reduction (Roden and Zachara, 1996, Lovely 1997, Bratina et al. 1998, Quantin et al. 2001). In contrast, for sulfate reduction, aqueous sulfate ions are converted to HS^- , which, in the presence of a suitable counter-ion, will precipitate as sulfide nanoparticles. Because reduction of sulfate is quantitatively linked to the oxidation of carbon, these metabolic pathways can generate copious quantities of nanoparticulate sulfides over short time periods (see **Figure 1a & b**).

In the absence of organic carbon for respiration and light for photosynthesis, both carbon fixation and energy generation can be driven by energy harvested from inorganic chemical reactions alone (Lovely 1993). In such chemoautotrophically based ecosystems, bacteria such as *Thiobacillus ferrooxidans* oxidize sulfide and/or ferrous iron that is present in pyrite (FeS_2) (Fowler et al. 1999). The resulting ferric iron and sulfate ultimately precipitate, often as nanoparticulate iron oxyhydroxide (ferrihydrite or

goethite, α -FeOOH) or iron sulfate compounds (schwertmannite, $\text{Fe}_{16}\text{O}_{16}(\text{OH})_y(\text{SO}_4)_z \cdot n\text{H}_2\text{O}$, and others).

Anthropogenic nanoparticles

Industrial manufacturing and combustion processes can lead to nanoparticle emission into the air or into wastewater effluent. For example, numerous groups are seeking to manufacture stable water-soluble magnetic iron oxide nanoparticles as an injectable diagnostic agent for enhancing contrast in magnetic resonance imaging (Tartaj et al. 2003). Cerium dioxide nanoparticles are of interest as catalysts during combustion processes (e.g., in automotive engines), because of the capacity of the CeO_2 lattice to buffer changes in oxygen partial pressures and oxidize carbon monoxide (Bekyarova et al. 1998). These nanoparticles may be released during manufacturing, use, or as the result of product disposal, and could ultimately accumulate in the environment in high enough concentrations to have important ecosystem impacts, such as accumulation in and toxicity for aquatic organisms (Oberdörster et al. 2005).

Impacts of nanoparticles on their surroundings

The formation of nanoparticles can influence the local chemical environment in which organisms live. Nanoparticles sequester ions when they precipitate, and can decrease or increase the porosity and permeability of sediments. For example, formation of sulfide nanoparticles removes both metal ions (e.g., Cu, Zn, As, Cd, Fe) and toxic sulfide ions from solution, improving habitability of the environment. Nanoparticle precipitation and dissolution reactions can be sources or sinks for protons, and thus can influence environmental mineralogy through the impact of pH on mineral solubility (Langmuir 1996). For example, the precipitation of iron oxyhydroxide nanoparticles and dissolution of sulfide nanoparticles both lead to environmental acidification, promoting dissolution of surrounding minerals. The solubilization of manganese oxides may liberate adsorbed trace metals that provide nutrients in oligotrophic environments (Bratina et al. 1998).

Nanoparticles, with their high surface areas, can play especially important roles in adsorption. For example, nanoparticles of iron oxyhydroxide formed during the neutralization of acidic, ferrous iron-rich solutions can sorb phosphate ions, possibly limiting biological productivity in some environments. Nanoparticle surfaces can also sequester protons or toxic ions such as arsenate (Waychunas et al. 2005).

Nanoparticles—Special properties and implications

Recently, a great deal of research has shown that nanoscale inorganic solids may exhibit substantially modified properties relative to their bulk counterparts (Alivisatos 1996, Murray et al. 2000, Trindade et al. 2001), with consequences for the inorganic and biological interactions of nanoparticles in the environment. As a foundation for studies of coupled geochemical processes involving nanoparticles, we examine some principles describing how size influences nanoparticle properties and reactivity. The present chapter introduces the physical and chemical consequences of small particle size in minerals, and discusses the effect small particle size has on redox and photochemical reactions. The concepts introduced here can be used for understanding the environmental impact and fate of both natural and engineered nanoscale materials.

Overview of small size effects in minerals

While molecular geochemistry has always been a “nano-science,” the science of nanoscale clusters and nanoparticles is distinct in an important way. The motivating tenet of contemporary nanoscience is that the chemical and physical properties of a solid inorganic material may vary as a function of particle dimensions below a critical size. The definition of the critical size depends both upon the material under consideration and the property of interest. It may refer to the start of a size dependent trend, such the onset of electronic confinement, or to an abrupt change, such as a switch in the thermodynamically stable structure of a mineral.

We stress that, in almost all cases, the description of the unmodified (i.e., bulk) material provides an excellent guide to the properties of a nanosized material (even below

a critical size). Thus, knowledge of the relevant solid state physics and chemistry for a given mineral is an indispensable foundation for understanding small-size effects. We emphasize, however, that important small size effects are not limited to modifications of nanoparticle structure and properties alone, which we denote as *static* effects.

Static small-size effects in mineral particles include the stabilization of structural phases that are metastable for bulk materials, and the presence elevated strain and disorder, particularly at nanoparticle surfaces. Electrons within solids respond to shifts in the equilibrium positions of atoms, surface-solvent interactions, and the presence of a confining surface itself. The latter effect—quantum confinement—is striking in some materials, but (when present) is neither the only, nor always the dominant, size effect in mineral nanoparticles. A large number of surface effects (e.g., confinement, surface charge, solvent interactions, and surface reconstruction) modulate electronic structure.

The kinetics of charge, energy, and material transfer also change at the nanoscale. Geochemical processes are *dynamic*, and significant size-dependent changes in reaction kinetics may affect processes in natural systems. The impact of nanoparticles on biogeochemical processes can depend on the kinetics of competing pathways. For example, the ability of photoexcited electrons in nanoparticles to reduce biomolecules is governed by the rates of several size-dependent processes that may enhance reactivity or dissipate energy without reaction. Furthermore, the products of various (photo)reduction experiments can be different for nano- versus micron-sized particles, indicating a size effect on reaction pathways (Müller et al. 1997).

We start by discussing small-size effects in individual particles. However, nanoparticles are frequently observed to be intimately aggregated, with significant consequences for their behavior in biogeochemical systems.

PHYSICAL STRUCTURE AND COMPOSITION OF NANOSCALE MINERALS

Thermodynamic constraints on the structure of nanoparticles

One of the better-understood ways that size can influence the structure of nanomaterials is through *interfacial energy* effects on phase stability. This topic was

reviewed in detail by Banfield and Zhang (2002) and Navrotsky (2002). In brief, when a compound can exist in more than one structural form (polymorph), a change in the relative stabilities of the structural variants may occur as the consequence of differences in their surface energies. This effect is only likely at small particle sizes, for which surface areas are large. For example, size-dependent phase stability may explain the precipitation of the hexagonal polymorph of ZnS (wurtzite) in place of the cubic form (sphalerite) in sediments or aqueous solutions, despite the higher stability of sphalerite compared to wurtzite in bulk materials up to temperatures over 1000 °C (Scott & Barnes 1972, Qadri et al. 1999, Zhang 2003).

However, it should be noted that kinetic effects may also lead to the production of metastable phases (amorphous or highly disordered materials), especially in low-temperature systems where precipitation rates are fast (Schwertmann et al. 1999, Wolthers et al. 2003). It can be difficult to assess whether an observed nanophase is thermodynamically stable or metastable. It can also be difficult to evaluate the structure and natural abundance of amorphous or highly disordered materials.

The nature of the initial precipitates and subsequent aging

For many minerals formed at low temperature or by biological processes, the initial precipitates are reported to be amorphous or highly disordered, possibly hydrated nanoparticles. Examples include amorphous iron sulfides, hydrous ferric oxide (HFO), and layered Mn(IV) oxides. These initial materials themselves do not grow beyond the nanoscale, and instead undergo crystallization, dehydration, or other transformations to mineral phases that may subsequently grow.

It is widely thought that extracellular bacterial surfaces provide sites for heterogeneous nucleation that lower the free energy barrier for precipitation (Fortin et al. 1997, Warren & Ferris 1998). This model is widely used to describe the precipitation of ferric iron as a result of the activity of iron oxidizing bacteria (Douglas & Beveridge 1998, Ferris 2005). The model is challenged, however, by a recent study of Rancourt et al. (2005), on the precipitation of HFO in the presence of nonmetabolizing bacteria. They showed that while Fe(III) ions adsorb onto functional groups on bacterial surfaces, they

remain external to the structure of HFO particles that subsequently form. Rancourt et al. argue convincingly that both inorganic and biological HFO formation *always* occurs via fast homogeneous precipitation.

There is also uncertainty as to the role of biological factors in affecting transformations that occur in nanoparticles after precipitation. While aqueous conditions (solution chemistry, pH, temperature), rather than their inorganic or biological origins, should govern the evolution of mineral precipitates (Konhauser 1998), comparative studies of the structure and reactivity of biominerals versus synthetic analogs frequently reveal differences. The presence of organic matter is thought to be a crucial factor (Ferris 2005). Furthermore, microbial metabolism frequently generates aqueous ions (e.g., Fe(II), or small organic molecules) that can interact with and stabilize or destabilize mineral surfaces during growth, phase transformation, and dissolution (Cornell & Schwertmann 1979, Urrutia et al. 1999, Davis et al. 2000, Thomas et al. 2004).

One interesting biological effect is the observation that the association of 2-line ferrihydrite nanoparticles with bacterial cell walls confers significant stability to the mineral against hydrothermal coarsening and transformation into hematite (Kennedy et al. 2004). The stabilization effect is observed with both biogenic and abiotic ferrihydrite in the presence of bacteria. It is inferred that the nanoparticles principally grow by an aggregation-based pathway that is hindered when the particles are immobilized on cell walls. Orientated aggregation (OA) is a significant pathway for nanoparticle growth in which individual particles achieve a common crystallographic orientation (Penn & Banfield 1998). Subsequent elimination of the interfaces between oriented particles can generate larger single crystals, some of which may have unusual morphologies and properties (Banfield et al. 2000). An example of joined UO₂ nanoparticles is given in **Figure 4**.

Size dependence of mineral solubility

From the point of view of biogeochemical systems, one of the most important size-dependent materials properties is solubility. As can be seen from the following

equation (Stumm and Morgan 1996), solubility increases as particle size decreases because the interfacial energy, γ , in J m^{-2} , is a positive contribution to the total energy.

$$\log K_{sp}' = \log K_{sp}^{BULK} + \frac{2/3\gamma}{2.3RT} S \quad (1)$$

In this equation, S is the surface area per mole, $R = 8.314 \text{ J mol}^{-1} \text{ K}^{-1}$ and T is the temperature in K. For ZnS, this equation predicts that the solubility of 3 nm particles of wurtzite is an order of magnitude higher than for bulk material at room temperature, assuming an effective surface area of $\sim 100 \text{ m}^2/\text{g}$, $\log K_{sp}^{BULK} = -22.85$ (Stumm & Morgan 1996) and $\gamma \approx 0.5 \text{ J m}^{-2}$ (Zhang et al. 2003). Sphalerite nanoparticles of the same dimensions are predicted to be two orders of magnitude more soluble, assuming $\log K_{sp}^{BULK} = -24.83$ and $\gamma \approx 0.8 \text{ J m}^{-2}$.

The accuracy of **Eqn 1** for quantitative predictions is limited. First, it assumes that interfacial energy is not itself size dependent, an assumption that has been questioned previously (Zhang et al. 1999). Second, accurate measurements of the interfacial energy are frequently unavailable, especially for hydrated surfaces that may additionally be coated by organic molecules. More realistic descriptions of the solubility of natural particles as a function of size, phase, and the surface chemical environment are needed.

Characterization studies of biogenic nanoparticles

We briefly review recent studies of the structure of important biogenic minerals. Precise structural characterization of biogenic nanoscale materials is challenging due to the small particle size, presence of disorder, and difficulties in isolating mineral precipitates from biomass. Powder x-ray diffraction (XRD) can be a convenient approach for determining nanoparticle structure, but has limitations. First, the width of peaks in diffraction patterns depends inversely upon the number of unit cells of material that make up the diffracting atomic planes. When the number of unit cells is very small (as in nanoparticles), peaks become extremely broad, obscuring structural details and the resulting diffraction pattern resembles those from materials with only short-range order.

Given these considerations, structure analysis based upon Bragg's law can be inaccurate at the smallest particle sizes (Palosz et al. 2002). Direct simulation of diffraction patterns from small structural models can be a more accurate method (Drits & Tchoubar 1990). Furthermore, when nanoscale particles possess significant disorder, XRD-based methods of particle size determination (e.g., via Scherer's equation, Patterson 1939) are extremely inaccurate (Wolthers et al. 2000). Pair distribution function (PDF) analysis of short-range order in nanoparticles is a promising extension of the powder XRD method (Gilbert et al. 2004, Billinge & Thorpe, 1998).

Nanoparticle imaging and structure analysis may be performed in the electron microscope by high-resolution transmission electron microscopy (HRTEM) and selected area electron diffraction (SAED). Bright, energy-tunable x-ray sources (synchrotrons) offer additional methods of structural and chemical analysis, including extended x-ray absorption fine structure (EXAFS), and x-ray absorption near-edge structure (XANES) spectroscopies. XANES spectra can be acquired with lateral resolution in scanning transmission x-ray microscopy (STXM) and x-ray photoelectron emission microscopy (X-PEEM). In addition, laboratory-based Mossbauer spectroscopy provides information on the chemical environment of the ^{57}Fe nucleus.

Iron oxides and oxyhydroxides

Biological and inorganic processes can lead to the precipitation of hydrous ferric oxides, as discussed above. Subsequent mineral transformations can produce nanocrystalline iron oxides including goethite or hematite (Benner et al. 2002, Hansel et al. 2003). Many environmental factors affect the mineral evolution. For example, low-temperature aging in the presence of water favors goethite formation; hematite is preferentially formed in warmer, dry environments (Cornell & Schwertmann 2003).

Magnetite (Fe_3O_4) is a common and mineralogically significant nanocrystalline iron biomineral product of the biological reduction of ferric iron. Dissimilatory iron reducing bacteria (DFeRB) utilize Fe(III) as an electron acceptor for the reduction of organic carbon (Lovely 1987, Bazylinski & Moskowitz 1997). HFO and crystalline ferric iron phases can provide a bioavailable source of ferric iron (Roden & Zachara, 1996). Fe(II) released from the mineral surface can re-adsorb onto unreacted HFO, forming

mixed-valence green rusts that age into nanoparticulate and poorly crystalline magnetite (Lovley et al. 1987, Sparks et al. 1990, Hansel et al. 2003). Alternative ferrous iron-bearing minerals may be formed, depending upon the aqueous flow rate, the relative concentration of HFO and the organic electron donor, and the presence of additional solution species such as phosphate and carbonate, and ferrous iron complexants (Urrutia et al. 1999, Roden et al. 2000, Hansel et al. 2003, Fredrickson et al. 2003). The rate of ferric iron reduction by *Shewanella putrefaciens* is correlated more with the surface area of the ferric iron substrate than the solubility of the particular ferric iron phase (Roden & Zachara 1996). However, differences in the solubility of crystalline (goethite and hematite) versus disordered (HFO) materials does affect the quantity and form of magnetite produced. Magnetite formation during the bioreduction of goethite and hematite is apparently limited to approximately 1 nm thick rinds on the initial ferric iron particles (Hansel et al. 2004), as shown in **Figure 2**. Similar mineral transformations are produced by Fe(II) adsorption onto synthetic iron oxides (Tronc et al. 1984, 1992).

Manganese oxides

Numerous microorganisms can enzymatically or indirectly facilitate the oxidation of aqueous Mn(II) by O₂ at far higher rates than inorganic pathways, although the biological function(s) of this activity is still unclear (Tebo et al. 1997, Tebo et al. 2004). Two recent studies of fresh biogenic material (from the bacterium *Pseudomonas putida* and from spores of the marine *Bacillus sp.* strain SG-1) reached similar conclusions on the structure of the first-formed product (Villalobos et al. 2003, Bargar et al. 2005). The material is a hexagonal phyllo-manganate assembled from stacked layers of Mn(IV) octahedra with considerable rotational stacking disorder (turbostratic disorder), plus a high negative structural charge due to Mn(IV) vacancies. (For a complete introduction to the complex crystal chemistry of manganese oxide materials, see Burns & Burns 1979, Villalobos et al. 2003, and Tebo et al. 2004.) These freshly formed biogenic minerals contained very little Mn(III). By contrast, aged biogenic oxides (Bargar et al. 2005) and Mn(IV) oxides found in soils were observed to have vacancies or Mn(IV) substitution by Mn(III) or heterovalent cations (**Fig. 3b**) (Isaure et al. 2005, Manceau et al. 2005). Mn(III) incorporation follows the autocatalytic oxidation of surface-sorbed Mn(II), which

is an important factor in abiotic transformation of the biogenic mineral. The precipitation and aging of biogenic Mn oxides is depicted in **Figure 3a**.

Sulfides

Transition metal sulfide minerals are common products of the metabolism of sulfate-reducing bacteria. In the case of iron sulfides, the first formed material is thought to be amorphous, but further growth and mineral transformation leads to the production of numerous crystalline phases (Wolthers et al. 2003, Benning et al. 2000). Observed biogenic iron sulfide minerals include mackinawite (tetragonal FeS), pyrite (cubic FeS₂), marcasite (orthorhombic FeS₂), greigite (Fe₃S₄) and pyrrhotite (Fe₇S₈). The exact mineral product is highly dependent on solution chemistry (Benning et al. 2000). It has been proposed that the sorption of ferrous iron to functional groups on cell surface membranes provides sites for heterogeneous nucleation, but as discussed above, sorption and precipitation processes may be independent. Iron sulfide minerals including FeS and FeS₂ are generally found to be sulfur deficient (Luck et al. 1989), but it is not known whether this is enhanced or suppressed in nanoscale particles. Disordered biogenic phases concentrated by magnetic separation were reported to have a high capacity for cation sequestration (Watson et al. 2000). Disordered nanocrystalline mackinawite exhibits an expanded lattice that incorporates water molecules, and possibly hydroxyl groups, cation impurity atoms, and sulfur vacancies (Wolthers et al. 2003).

Even in the presence of ferrous iron, alternative minerals may precipitate if thermodynamically favored. Labrentz et al. (2000) observed that highly pure ZnS nanoparticles are formed in close proximity to sources of dissolved ferrous iron. A common feature of biogenic ZnS nanoparticles is the presence of stacking faults and wurtzite nanoparticles, probably reflecting the low free-energy difference between the sphalerite and wurtzite phases (**Figure 4**, and see Moreau et al. 2004). Interestingly, recent studies on synthetic mixed-phase ZnS nanoparticles have indicated a significant effect on the profile and size of the semiconducting band gap (H. Zhang, personal communication).

Other minerals

The reduction of U(VI) in the aqueous uranyl ion (UO_2^{2+}) to form insoluble uraninite (UO_2) nanoparticles can take place as a by-product of microbial metabolism involving sulfate (**Figure 4**; Suzuki et al. 2002) or iron reduction (Lovely et al. 1991, Fredrickson et al. 2000). Uraninite nanoparticles can also form abiotically following the reduction of uranyl by ferrous iron (O'Loughlin et al. 2003).

Suzuki et al. (2002) used HRTEM to document the presence of biogenic UO_2 nanoparticles as small as 1 nm in diameter, and EXAFS spectroscopy to infer that the average particle size is ~ 1.5 nm. Given the presence of 2–4 nm particles, this result suggests that ultra-small particles or molecular clusters are abundant. The U-O bond length exhibited a 0.007 nm contraction relative to bulk UO_2 , indicating the presence of significant surface strain, and an associated increase in solubility. By estimating a relationship between surface stress and interfacial energy, and assuming negligible size-dependent changes in compressibility, this observation was used to predict a billion-fold increase in the solubility of biogenic uraninite relative to the bulk mineral. The uncertainties in the assumptions required for this calculation emphasize the need for additional studies on nanoparticle structure, elastic properties, and solubility.

The effects of water and other surface-bound molecules on nanoparticle structure

As the medium in which minerals form, water itself is a key player at every stage in the precipitation and evolution of nanoparticles at and near the Earth's surface. Rapid precipitation pathways frequently lead to structural incorporation of water molecules. While the interactions between water and bulk mineral surfaces have been an area of intense study (Hochella & White 1990, Henderson 2002), there are relatively few structural or calorimetric studies on solvent interactions with nanoparticle surfaces (but see Navrotsky, 2004). Nevertheless, it has been shown that nanoparticle surface interactions with water can be strong and decisive in stabilizing particular mineral structures. Diffraction studies in controlled environments have shown that surface hydration is an important factor in the surface and interior structure of ZnS and $\gamma\text{-Fe}_2\text{O}_3$ nanoparticles (Zhang, Gilbert et al. 2003, Belin et al. 2004). In these examples, changes in surface hydration caused dynamic structural responses in the nanoparticles.

Zhang, Gilbert, et al. (2003) demonstrated that adsorption of water drove a structural transformation in ZnS nanoparticles at room temperature without any change in particle size. The water-driven reaction was not reversible. However, the desorption and re-adsorption of a more volatile solvent (methanol) does cause reversible structural changes, and it is inferred that the activation barriers for structural rearrangements in these nanoparticles are small enough that they can be overcome by surface interactions at room temperature.

The findings from the study of ZnS nanoparticles do not imply that natural nanoparticles will always find their energy minimum state, given their size and surface chemical environment. But they do emphasize that the dynamic response of the atoms in a nanoscale particle will permit this under certain circumstances.

Other groups have sought a description of the phase stability of mineral nanoparticles, based upon surface interactions in the framework of equilibrium thermodynamics. It was recently argued that, because of the high surface area of nanoparticles, the adsorption of hydroxyl groups or oxyanions onto HFO nanoparticles represents a significant change in the stoichiometry, one that can affect the thermodynamic stability of the nanoparticle-sorbate system (Fukushi & Sato, 2005). Vayssières et al. (1998) interpreted the pH dependence of the phases of iron oxide nanoparticles synthesized with aqueous methods to indicate that the enthalpy of surface adsorption is a governing thermodynamic contribution. Lodziana et al. (2004) have used molecular simulations to describe the very high stability of the hydroxylated θ -Al₂O₃ (110) surface as a thermodynamically stabilized (i.e., negative interfacial energy) material. However, such characterizations remain controversial, because in the absence of clearly reversible transitions it is difficult to assess whether the observed material is the true thermodynamically stable state.

The observations that surface ligands can direct the structure of a nanomaterial may be directly relevant to low-temperature biogeochemical systems. In these environments, small mineral particles are closely associated with solute molecules including small organic compounds, and high molecular weight polymers including proteins and polysaccharides. These compounds may represent a biological influence on the structure of nanoparticles in aqueous systems. In general, molecular simulations that

have incorporated realistic surface-solvent or surface-ligand interactions have revealed strong interactions that stabilize both the surface and interior structure of nanoparticles (Rabani, 2001, Pokrant & Whaley, 1999, Zhang et al. 2002, Kerisit et al. 2005).

Incorporation of impurity atoms

Contaminants (e.g., Zn, As) and nutrients (e.g., phosphate) are readily adsorbed on, co-precipitated with, and incorporated into mineral nanoparticles (Watson et al. 2000, Gunnars et al. 2002, Hochella et al. 2005a,b) and (photo)redox cycles of nanoscale iron and manganese oxides and oxyhydroxides can cause the incorporation and release of these species (Isaure et al. 2005). Since it is widely observed that the availability and transport of aqueous ions is highly correlated to their interactions with colloidal particles (Kimball et al. 1995, Brown et al. 1999), important aspects of nutrient and contaminant biogeochemistry depend on their association with mineral nanoparticles. Furthermore, the reactivity of the nanoparticles themselves can be strongly modified by the incorporation of even low concentrations of impurity atoms. For example, the incorporation of 0.2 mol% Zn into pyrite drastically affects surface photochemical behavior, with no detectable structural modifications (Büker et al. 1999). As explained below, impurity atoms can introduce additional electronic energy levels that can affect mineral reactivity.

An understanding of the factors controlling impurity atom incorporation in nanoparticles remains incomplete, both in the materials and earth sciences. As with bulk materials, the ability of nanoparticles to host impurities depends on the structural characteristics of the solid, the size and charge discrepancy between the impurity and intrinsic ion, and the response of the structure to the structural perturbation associated with ion incorporation (Fistul 2004, Cornell & Schwertmann 2003). Careful combined x-ray absorption, x-ray diffraction and structure modeling studies are required to elucidate the crystal chemistry of incorporated atoms in disordered minerals (Isaure et al. 2005, Manceau et al. 2005)

Defects such as ion substitutions or vacancies have an associated enthalpy from which their mean concentration can be calculated, assuming thermodynamic equilibrium. However, distributing the same number of defects in nanoparticles rather than bulk

material would result in the vast majority of nanoparticles being defect-free. Furthermore, there may be an impurity exclusion effect, as solid-state diffusion times to the surface are likely to be quite short (Tang et al 2003). Consequently, the presence of detectable impurity concentrations in nanoparticles is likely to indicate favorable kinetic pathways, rather than thermodynamic equilibrium.

An important advance in modeling and predicting impurity incorporation is the recent proposal that it is the affinity of dissolved impurity ions for the surface of a growing nanoparticle that is the key factor determining eventual incorporation (Erwin et al. 2005, commentary by Galli 2005). The excess energy of the impurity once it is in the host lattice is not the dominant factor. Rather, it is the rate of impurity adsorption and desorption at specific surface sites relative to nanocrystal growth kinetics. The implication is that the fast precipitation reactions that follow microbially mediated changes in the oxidation state of environmental ions such as iron, manganese and sulfur might be effective at scavenging reactive aqueous species.

There is considerable empirical evidence for significant impurity concentrations in natural nanoparticles. For example, disordered Mn(IV) and Fe(III) oxides and oxyhydroxides are commonly observed to account for the majority of transported contaminant ions (Hochella et al. 2005). Certain impurity atoms can affect the phase stability or enhance the crystallinity of biominerals (Davis et al. 2000, Webb et al. 2005).

It is of interest to determine whether the miscibility of substances that form solid solutions is affected by small particle size. For example, bulk ferric iron oxides can accommodate homovalent cation substitution (e.g., Cr^{3+} and V^{3+}) to 5–10 mol% (Schwertmann et al. 1989, Schwertmann & Pfab 1994), and bulk $\text{Zn}_x\text{Fe}_{1-x}\text{S}$ forms a solid solution for all values of x (Vaughan & Craig 1978). There are presently no investigations into the stability of these materials as nanoparticles. Most effort has been directed to the production of technological materials. In particular, the introduction of Fe^{3+} and Cr^{2+} into TiO_2 nanoparticles creates photocatalysts with higher yields (Zhang et al. 1998, Bryan et al. 2004), and the doping of Mn^{2+} into ZnS nanoparticles enhances their luminescence efficiency (Yu et al. 1996).

The surfaces of nanoscale minerals

The surfaces of materials have many distinct structural and electronic properties relative to the bulk or the interior. Surfaces host, mediate, or participate in all relevant biogeochemical processes involving minerals. Decades of surface science provided considerable knowledge about mineral surface structure and surface chemical interactions. However, all such work has been performed on the surfaces of bulk minerals, and it can be argued that the surface science of nanoscale minerals is just beginning.

It might be reasonable to expect, *a priori*, that the constituents of nanoparticle surfaces will include facets and defects (such as edges or vertices) very similar to those found on bulk mineral surfaces, perhaps with a few additional types. However, the results of certain experimental and theoretical studies indicate that this model may be seriously misleading. Zinc sulfide nanoparticles in the 1–5 nm diameter size range are observed to possess significant interior distortion, which is inferred to be provoked by extreme reconstruction at the surface (Gilbert et al. 2004). This model is supported by molecular dynamics calculations showing highly distorted surfaces that, because of high surface curvature, bear little resemblance to facets of bulk minerals (see **Fig. 5**). Large-scale molecular simulation of goethite nanoparticles within a dissociating model of water, and with dimensions below 10 nm, accumulate protons at highly charged edge sites to a far greater extent than is anticipated from models with simple slab geometries (**Fig. 5**) (Rustad & Felmy, 2005). Nanoparticle surfaces may additionally be stoichiometrically distinct from the interior, as has been determined recently for the surfaces of bulk hematite (Glenn Waychunas, personal communication).

Also, partial transformation caused by surface oxidation or reduction can lead to the formation of maghemite ($\gamma\text{-Fe}_2\text{O}_3$) layers on magnetite surfaces, and magnetite films on HFO or hematite (cf. **Fig. 2**) (Hansel et al. 2004).

Studies of the mechanism and geometry of adsorbate binding to nanoparticle surfaces are one approach to compare the surfaces of bulk and nanocrystalline minerals. Mercury, arsenic, and copper are known to attach to the surface of goethite ($\alpha\text{-FeOOH}$) via inner sphere coordination and thus are suitable test sorbates for goethite nanoparticles. The coordination environment of Hg adsorbed to 5 nm diameter goethite

nanoparticles is modified relative to sorption sites on larger particles, with an expansion of the 2nd and 3rd shell He-O and Hg-Fe distances (Waychunas et al. 2005). However, no significant size-dependent changes in the sorption geometry of As(V) or Cu(II) were detected.

At present, there is no general framework for describing nanoparticle surfaces, and both practical and theoretical approaches require considerable development. Modern x-ray methods that probe the structure of water and the chemistry at mineral surfaces must be adapted to the surfaces of nanoparticles (Eng et al. 2000, Cheng et al. 2001).

ELECTRONIC STRUCTURE OF NANOSCALE MINERALS

Introduction to electronic structure of solids

Electronic structure is key to the reactivity of materials. The electrochemical potential of electrons in solids drives chemical reactions that underpin many of the Earth's biogeochemical cycles. Thus, we begin this section with an introduction to the electronic structure of solids in a form that will permit size-dependent effects and molecular scale reactivity to be addressed. The quantum theory of solid-state materials gives the best quantitative description of electrons in solids and is presented in numerous texts (Ashcroft & Mermin 1976). It is briefly recapped here with an emphasis on the analogies between bonding in molecules and in periodic crystals.

Approximate descriptions of electrons in solids

The enormous number of atoms and electrons in solids renders exact solutions of electronic and nuclear motion utterly intractable, and requires drastic simplifying assumptions. The following are two of the most important. First, the nuclear motion is considerably slower than electronic motion, and hence the nuclei are assumed to be static during calculations of electronic structure. Second, the behavior of only a single electron is considered, with an averaged description of the influences of all other electrons and nuclei. Within the framework of this single-electron approximation, Schrödinger's Equation can be written:

$$[E_k + V(\mathbf{r})]\psi_i(\mathbf{r}) = E_i\psi_i(\mathbf{r}) \quad (2)$$

Eqn 2 relates the total energy, E_i , and wavefunction, $\psi_i(\mathbf{r})$, of an electron in a state i to its kinetic energy, E_k , and to the potential, $V(\mathbf{r})$, within which it moves. The potential energy term principally contains the electrostatic potential of each atomic site, and defines the energy landscape in which the electron moves. An important additional contribution to $V(\mathbf{r})$ describes (approximately) the correlated interactions with all other electrons. Collectively, the energy terms are called the *Hamiltonian*, H , which completely defines the possible electronic states for a given system. The wavefunction is the most complete description attainable for a quantum particle and represents the probability of finding the particle within an infinitesimal volume of space.

The simplest model of size effects on electronic structure relies on the description of an electron traveling freely in space. For a given electron momentum, described using the wave vector k , the energy of a free electron is given by

$$E = \frac{\hbar^2 k^2}{2m_e}, \quad (3)$$

where m_e is the mass of the electron and $\hbar = h/2\pi$, where h is Planck's constant. For numerous materials, the electrons that participate in chemical reactions can be considered as free electrons, but with a modified effective mass, m_e^* . The effective mass captures the effect of the periodic structural environment on the propagation of wave-like electrons within the material. Assuming that the mobility of an electron in a material does not vary with particle size, m_e^* is obtained from a first-principles calculation of the electronic structure of a bulk material (i.e., by obtaining the solutions of **Eqn. 2**).

Solutions of Schrödinger's Equation

There are two important concepts that permit effective solution of the single electron Schrödinger's equation for bulk materials. First is the realization that the solution wavefunctions (or orbitals) possess the same symmetry as the spatial distribution

of atoms with which they are associated. Atoms (and hence the wavefunctions of atomic electrons) possess spherical symmetry. Orbitals that are centered on atoms in a molecule possess the point symmetry of that site; and, as bulk crystals fill space with identical unit cells, the electronic wavefunctions of periodic crystals possess translational symmetry. The last statement is known as Bloch's theorem, and provided the foundation for an explosive growth in solid-state physics during the 20th century. The second principle is that a wavefunction can be expressed as a linear combination of any set of basis functions that are mathematically complete. This is exactly analogous to the use of Fourier series to represent an arbitrary function. An example of this approach is molecular orbital theory, in which a linear combination of atomic orbitals is used to describe new electronic states formed when atoms bond. It permits the efficient numerical simulation of electronic structures, because realistic electronic wavefunctions can be built up as a combination of computationally convenient basis functions.

As wavefunctions are (in principle) independent of the choice of basis functions, there is an equivalence between choices. This can be seen by comparing the results of real-space cluster calculations and momentum-space band-structure calculations for the same mineral. Band structure calculations give similar results for the energy positions of electronic levels (bands) in solids that can be derived from cluster calculations, but additionally show how the energy-momentum relation varies with direction of travel in a crystal. An example for sphalerite, the cubic modification of ZnS, is given in **Figure 6**. The bulk electronic structure of a material is the starting point for understanding the properties and reactivity of nanoparticles of that material.

Energy levels in semiconductor minerals

An important focus of this chapter is the role that nanoparticles play in redox reactions in biogeochemical systems. It is necessary, therefore, to introduce the concepts used to describe the behavior of electrons in bulk and nanosized systems. With a few exceptions, biogenic minerals are semiconductors or insulators.

The valence and conduction bands and the band gap

The valence band (VB) and conduction band (CB) in solids are the exact analogs of the highest-occupied molecular orbitals (HOMO) and lowest-unoccupied molecular orbitals (LUMO) in molecules. The **Fermi energy**, E_F , can be considered the electronic electrochemical potential within the material. For insulators and semiconductors, E_F lies between the (completely occupied) VB and (empty) CB.

When a valence electron is excited (by thermal energy or by light absorption) and acquires sufficient energy to jump to the conduction band, a charge deficit, or hole, is created in the VB that acts just like a mobile positive charge. The electronic **band gap** is the energy required to excite an electron into the conduction band and move it out of the electrostatic field associated with the hole that is created. The spatial scale that defines this distance is the **Bohr radius**, the radius of the lowest-energy bound state of an electron-hole pair that are mutually attracted because of their opposite electrostatic charges. Such a bound pair is called an **exciton**.

The conductivity of minerals

Electronic conductivity requires mobile charge carriers in bands that are not completely occupied. Energy bands in solids are occupied with electrons up to the Fermi level. Hence, at zero temperature, metallic behavior is expected in a pure solid if the Fermi level lies within a band, while insulating behavior is expected if it lies between bands. At higher temperatures, and for sufficiently small band gaps, thermal energy can excite electrons in the vicinity of the Fermi level. The promotion of a small number of electrons to the conduction band can enable conduction via both CB electrons and the associated VB holes. Pure materials that conduct by this mechanism are called **intrinsic semiconductors**. For some crystal structures, electronic transitions between the top of the VB and the bottom of the CB require exchange of momentum between the electron and vibrations of the lattice (phonons). Materials in which excitation across the band gap is phonon-assisted are called **indirect** semiconductors.

Solids in which bonding arises from the interactions of *s* or *p* atomic levels follow the above description closely. However, other materials are anticipated to be metallic according to the above criteria, but are measured to be very poor conductors (Cox, 1992). This is because when bonding involves partially occupied *d* or *f* levels, two additional

factors can limit electron and hole mobility. First, low overlap between atomic orbitals of neighboring atoms can lead to the localization of outer shell electrons on a single atomic site. Second, energetic barriers may exist that limit charge transfer between neighbors. The origins of such barriers may be associated with electron repulsion or correlation energies, or may be structural. There is a continuum from highly *localized* to highly *itinerant* electronic behavior within which many environmentally relevant transition metal oxides and chalcogenides fall. In numerous iron-bearing materials, magnetic ordering of electrons below a threshold temperature can abruptly change the electronic properties from those of an itinerant semiconductor to localized insulator. Even for some bulk minerals such as hematite (Fujimori et al. 1986) and magnetite (Park et al. 1997, Todo et al. 2001), controversy remains with regard to the nature of the VB and CB electronic states. These distinctions, and controversies, persist in nanoscale particles.

An additional important class of materials are the *extrinsic semiconductors*. Impurity atoms or point defects can provide electronic states within the band gap of an insulator or intrinsic semiconductor. The energy required to excite electrons or holes to or from these states can be significantly lower than transitions across the full band gap. Consequently, even very low concentrations of impurities can dominate the conductivity of bulk minerals. The charge carriers introduced into a solid by impurities or defects can be itinerant or localized just as the carriers introduced from atoms intrinsic to the material. Consequently, the incorporation of impurities during nanoparticle nucleation and growth can have a significant effect on reactivity.

Many of the partly occupied *d*-shell configurations found in iron- and manganese-bearing compounds have associated magnetic properties. A review of nanoscale magnetism is given by Rancourt (2002).

Electron hopping conduction mechanisms.

Localized electrons or holes experience an energy barrier against transfer to neighboring atomic sites, but at finite temperatures the thermal energy of the system may be sufficient to overcome the barrier. Thus, localized charge carriers can be mobile through a “hopping” mechanism from site to site. An important example is that of the *small polaron*, an electron or hole that is transiently trapped at each site because of the

distortion of the immediate lattice that it provokes, and which follows it. As with any process with an activation energy barrier, mobility increases with increasing temperature.

A theoretical treatment of hopping conductivity (Cox 1992, Rosso et al. 2003) originated from a model electron-transfer reactions between ions in solution (Marcus 1993, Barbara et al. 1996), and is also applicable to charge and exciton transfer between nanoparticles (Adams et al. 2003; see below). Quantum mechanical *tunneling* is an alternative mechanism that may dominate for acceptor-donor distances less than 14 Å, and is utilized by many proteins and electron shuttles (Moser et al. 1992, Page et al. 1999). Tunneling processes do not pass through an intermediate higher energy state and are therefore distinct from the hopping mechanism.

Consider the transfer of an electron from a donor (D) to an acceptor (A). The donor could be a reductant in solution or a site in a crystal that has trapped an electron.



The rate of electron transfer, k_{et} , has an Arrhenius-type dependence:

$$k_{et} = \kappa \nu \exp\left(-\frac{\Delta G^*}{k_B T}\right), \quad (5)$$

where ΔG^* is the Gibbs free energy of an intermediate state (the *activation energy*), k_B is Boltzmann's constant, and κ is a prefactor for a given system. Thermal motions of the atomic nuclei bring the system into the most favorable configuration for charge transfer with a certain frequency, given by ν . In the intermediate state, the electron overlaps with both the donor and acceptor. The major contribution to the activation energy is the *reorganization energy* associated with the geometry of the intermediate state. The activation energy also includes electrostatic interactions between the electron and the atoms or molecules that coordinate the donor and acceptor, such as near-neighbor atoms in a crystal or hydrating solvent molecules.

Hopping-based conductivity in minerals is generally highly anisotropic, as determined by the crystal structure and electron spin ordering. For example, conduction

in hematite occurs predominantly along the (001) basal planes (Rosso et al. 2003). Conduction in magnetite involves the octahedral sites on which Fe(II) and Fe(III) ions are distributed to the exclusion of purely Fe(III) tetrahedral sites (Cox, 1992). As motion of the atoms is required for the system to reach the intermediate state, modifications in the vibrational properties of nanoparticles at small size (e.g., Gilbert et al. 2004) may significantly affect charge (or impurity) transport.

Electronic structure of nanoparticles

Pure size-dependent modifications of electronic structure substantially depend on the extent to which the valence electrons are delocalized. When the dimensions of a semiconductor are similar to the Bohr radius, an electron and hole can never be so far apart that the interaction between them can be neglected. Consequently, the lowest energy excitation is not equivalent to the bulk band gap, as defined above, but contains additional terms, principally the (positive) confinement energy and the (negative) electron-hole Coulomb interaction. The confinement energy dominates and the nanocrystal exhibits an increase (or blue-shift) in its band gap. Band gap opening is readily observed with ultra violet–visible (UV-vis) absorption spectroscopy, but the individual shifts of the VB and CB are not obtained with this approach. Combined x-ray absorption and x-ray emission spectroscopies can resolve the size dependent trends in the energy positions of the occupied and unoccupied bands (**Figure 7**).

The electronic structure of bulk materials with delocalized electrons is well modeled by band structure methods (using translation symmetry). It is obvious, however, that even the most crystalline nanoparticle lacks long-range periodicity. To date, two approaches have been adopted to deal with this.

Effective Mass Approximation (EMA)

Virtually all geochemically relevant optical and redox behavior of materials involves the charge carriers in the vicinity of the top of the VB or the bottom of the CB. (The region of interest is circled in **Figure 6**.) The effective mass approximation (EMA) is an approach that describes how a perturbation in a material (such as finite size) affects

these electrons and holes, disregarding all others. It assumes that the mobility of electrons and holes (represented by the effect mass, and determined by the crystal lattice) is unchanged in nanoparticles. The size-dependent shifts in absolute energy positions of the VB and CB are given by the confinement energy of a hole and electron, respectively.

The simplest EMA theory considers an infinite confining potential at the nanoparticle-solvent interface. Simple analytical expressions are obtained for spherical nanoparticles of radius d :

$$E_{VB}^{\infty}(d) = E_{VB}^0 - \frac{2\hbar^2\pi^2}{d^2 m_{h,in}^*}; \quad E_{CB}^{\infty}(d) = E_{CB}^0 + \frac{2\hbar^2\pi^2}{d^2 m_{e,in}^*} \quad (6)$$

In this expression, E_{CB}^0 and E_{VB}^0 are the CB and VB energy positions for the bulk material, and $m_{e,in}^*$ and $m_{h,in}^*$ are the effective masses of the electron and hole inside the nanoparticle. Brus (1984) was the first to consider quantum confinement effects on the redox potential of nanoscale solids, and his predictions for CdSe with an infinite potential are shown in **Figure 8**.

The energy step at the interface must result from either the electron affinity of a solid (~ 5 eV) or the band gap of the surrounding medium (3.8 eV for aqueous systems, Memming 2001). Several authors have shown that a significant quantitative improvement to the EMA is obtained when a finite confining potential is considered (e.g., see **Figure 7**) (Tran Thoai et al. 1990, Schoos et al. 1994, Lüning et al. 1999). Exact analytical expressions are no longer obtained, and electron and hole energies are generally obtained numerically. However, Ferreyra & Proetto (1999) provide an approximate expression for the confinement energies in a finite confining potential. For a spherical particle of diameter d and a confining potential V_{out} outside:

$$E_{VB}(d) = E_{VB}^0 - E_{VB}^{\infty}(1 - \delta_h); \quad E_{CB}(d) = E_{CB}^0 + E_{CB}^{\infty}(1 - \delta_e) \quad (7)$$

where $\delta_e = \hbar/d m_{e,in}^* \sqrt{8m_{e,out}^*/V_{e,out}}$, with an equivalent expression for δ_h . For particles in water or air, it is generally assumed that $m_{e,out}^* = m_{h,out}^* = m_e$, the mass of the free electron. Holes are perfectly confined, so that $V_{h,out} = \infty$ and $\delta_h = 0$.

In the so-called strong confinement regime (for nanoparticle radius similar to or less than the Bohr radius), the electron and hole can be considered as individual particles. Then the band gap is obtained from difference in the size dependent VB and CB energy positions, plus the additional term resulting from the electrostatic interaction of the electron and hole pair. The band gap, E_g , for the same particle considered above is:

$$E_g(d) = E_g^0 + \left\{ \frac{2\hbar^2\pi^2}{d^2} \left[\frac{1}{m_{e,in}^*} + \frac{1}{m_{h,in}^*} \right] - E_e^\infty \delta_e - E_h^\infty \delta_h \right\} - 3.6 \frac{e^2}{\epsilon d} [1 - (\delta_e + \delta_h)/4] \quad (8)$$

where e is the charge on an electron and ϵ is the high frequency dielectric constant of the bulk semiconductor. In this expression, E_g^0 is the band gap of the bulk, the second term considers the kinetic energy of the electron and the hole (i.e., the confinement energy – this is an alternative version of **Eqn 7**) and the smaller third term is the Coulomb attraction between electron and hole (see discussion in Nanda et al. 2004). Effective mass values may be found directly in the literature (e.g., Landolt-Bernstein 1983) or estimated from band structure calculations (e.g., Edelbro et al. 2003).

Limits and Extensions of the EMA

The EMA tends to overestimate the band gap in quantum confined materials, even when a finite confining potential is used, an effect that is exacerbated at the smallest sizes. Consistent values for the effective mass can be hard to obtain from the literature; however, the EMA is only weakly dependent on the precise values for the effective mass (Gaponenko 1998, Pelligrini et al. 2005).

The EMA is believed to be valid for both direct and indirect semiconductors. Absorption measurements on indirect semiconductors have shown that they retain this characteristic property down to very small sizes (~100 atoms; Delerue et al. 2001) and that confinement effects on band edge positions and band gaps are similar to those in

direct semiconductors (Tolbert et al. 1994). However, the UV-vis absorption edge is generally not sharp for the indirect semiconductors, and even for well studied materials such as TiO₂, this transition (which reveals the true band gap) has been confused with stronger, direct transitions to higher-energy CB states (Serpone et al. 1995, Monticone et al. 2000).

The EMA assumes that there are no size-dependent changes in particle structure, but changes in structure may overwhelm confinement effects in wide band-gap, low-mobility materials. Furthermore, in narrow-band-gap semiconductors, such as PbS ($E_g = 0.41$ eV), the band edge states are not well approximated as free electrons, and hence quantitative agreement is poor. In such cases, the EMA underestimates the band gap (Pellegrini et al. 2005). Additional refinements of the EMA approach have been performed. Examples include the treatment of multiple bands in the VB and CB (Efros & Rosen, 2000), and inclusion of surface polarization terms (Brus, 1986). Nanda et al. (2004) discuss variations of the finite potential EMA for nanoparticles with slab (2D) and rod (1D) geometries.

Many of the above methods assume that important material constants for nanoparticles, such the dielectric constant or the effective mass of the relevant charge carrier(s), are unchanged relative to bulk materials. These assumptions are presently untested. However, recent calculations indicate that the dielectric response of a material change very little with decreasing size, with the exception of small near-surface effects (Cartoixa & Wang, 2005).

Real-space cluster models

As discussed above, band structure and real-space depictions of electronic structure are highly complementary approaches. Real-space methods discard all assumptions of symmetry and are thus suited to nanoparticles. However, they carry a significant price, because whole-nanoparticle simulations must treat hundreds of non-equivalent atoms, while band-structure calculations consider only the number of atoms in a unit cell.

The most important input to a cluster calculation is the atomistic real-space structural model itself. Nanoparticle structures are generally assembled by hand, or with

classical molecular dynamics structure optimization, and the uncertainty in the structures derived in these ways are a major limitation for subsequent electronic structure calculations, no matter how sophisticated. The nature and structure of nanoparticle surfaces remain particularly obscure, because no experimental method is presently able to directly visualize it. Obviously, uncertainties surrounding the true structures of nanoscale materials cause equally great uncertainties in anticipating their electronic properties.

Nevertheless, atomistic simulations provide the clearest visual depictions of nanoparticle structure (Rabani, 2001, Pokrant & Whaley, 1999) and have played an invaluable role in evaluating theoretical approximations such as the EMA (Lippens & Lannoo, 1987, Wang & Zunger, 1996, Franceschetti & Zunger, 1997). Simulations that are performed with care are experiments *in silicio*, useful for evaluating and predicting mechanisms or trends in behavior that can be tested experimentally (Zhang, Gilbert et al. 2003, Rustad & Felmy, 2005, Kerisit et al. 2005, Erwin 2005). Real-space cluster calculations will prove essential for understanding the electronic structure in complex environmental nanoparticles for which simple models such as the EMA are not applicable (O'Connor & Sposito, 2004).

Ideally, electronic and physical structure would be simultaneously optimized, as implemented by the Car-Parinello method (Car & Parrinello, 1985, Galli & Parinello, 1992). The “Quantum Monte Carlo” simulations by the Galli group have demonstrated the value of this approach for showing the effects of surface reconstructions on the electronic structure of nanoclusters (Puzder et al. 2003). However, nanoparticles of diameter greater than ~ 2 nm remain large even for efficient first-principle calculations.

Solvent effects on nanoparticle electronic structure

An interesting consequence of a finite confining potential is that tails of the electron or hole wavefunctions extend into the medium surrounding the particle, as depicted in **Figure 9**. This generally has a slight effect on the energies of the electron and hole states. However, solvents with a high dielectric constant can stabilize nonuniform charge distributions at the surface (Rustad & Felmy 2005), enhancing the strength of dipolar interactions between nanoparticles (Rabani 1999) and can permit solvent-mediated conductivity (Brus 1996), as discussed below.

The simplest approach for estimating solvent effects on electronic energy levels in nanoparticles is to treat the solvent as a continuum characterized by a dielectric constant (Qu & Morais, 1999, Rabani et al. 1999, Franschetti et al. 2000). However, it is clear from decades of research on mineral-water interfaces that a continuum description of water is severely limited (Hochella & White, 1990). In fact, we require a much more complete description of the nanoparticle–electrolyte interface.

Interfacial electrochemistry of nanoparticles

When a solid material is immersed in an electrolyte such as water, redistribution of charge carrying species occurs on both the solid and liquid sides of the interface. This process can produce significant shifts in the absolute energy positions of electronic states at the interface, and hence affect the redox properties of the bulk mineral or nanoparticle.

When the two phases touch, the system as a whole reaches thermodynamic equilibrium by equating the *electrochemical potentials* for all species in the material and the electrolyte. As introduced above, the electrochemical potential for an electron in a semiconductor is equal to the Fermi energy, E_F , which lies between the valence and conduction bands. The electrochemical potential associated with the electrolyte is related to the redox potential of the system. The half reaction for a redox reaction in the electrolyte can be written:



The reduced and oxidized species in **Eqn 9** are alternate states of a single system in which an electronic orbital is occupied or unoccupied, respectively. The electronic energies of these states are not equivalent because the solvent cannot reorganize to a ground state configuration on the time-scale of electron transfer reactions, and $E_{Ox} > E_{Red}$. Thus, the reduced and oxidized states of the redox system are analogous to the occupied (valence band) and unoccupied (conduction band) states in a solid, and we may define an effective Fermi energy for the solution, $E_{F,redox}$, that lies midway between E_{Ox} and E_{Red} . (Gerischer 1970).

The electrochemical potential, $\bar{\mu}_i$, of an ion, electron, or other species, i , is equal to its chemical potential, μ_i , plus an additional term for each charged species if it resides within an electric field.

$$\bar{\mu}_i = \mu_i + z_i F \phi \quad (10)$$

The additional energy term is the product of the charge on the species, z_i , the local electrostatic potential, ϕ , and Faraday's constant, F . The relation between the chemical potential, μ_i , and the activity of ion i is given in many textbooks (Lyklema 2001). The electrochemical potential for the electron in **Eqn 9** is defined as the difference in the values for the oxidized and reduced species, $\bar{\mu}_{e,redox} = \bar{\mu}_{Red} - \bar{\mu}_{Ox}$. (Memming 2001). The electrolyte Fermi energy, $E_{F,redox}$ (in eV), is then related to $\bar{\mu}_{e,redox}$ (in J mol⁻¹), by

$$E_{F,redox} = \frac{e}{F} \bar{\mu}_{e,redox}. \quad (11)$$

For the solid phase and aqueous phase Fermi level concepts to be directly comparable, they must be expressed in the same units on the same energy scale, typically in eV on the absolute vacuum scale (AVS). The redox potential associated with a half reaction such as **Eqn 9** is usually expressed in V relative to the normal hydrogen electrode (NHE) or other electrode. As discussed by Xu & Schoonen (2000), the energy of an electron in an energy band can be converted to the associated redox potential by the relation

$$E(\text{NHE, V}) = -E(\text{AVS, eV}) - 4.5. \quad (12)$$

At equilibrium, $E_F = E_{F,redox}$, which requires charge redistribution. Electrons flow into the solution from the material and change the concentration of redox species if $E_F > E_{F,redox}$, and vice versa. This changes the potential at the interface, lowering the

free-energy difference due to the term $z_i F \phi$ in **Eqn 10** until equilibrium is attained. The VB and CB states at the interface are affected by the local potential, a phenomenon called **band bending**, as depicted in **Figure 10**. Energy levels further from the interface than the Debye length, L_D , are shielded from the effect of the interfacial potential because of the dielectric properties of the solid. L_D is typically greater than 100 Å, depending on the density of charge carriers. Thus, surface charges are not well screened in particles of dimensions smaller than this, and the electronic bands are flat (but shifted) throughout a nanoparticle, as illustrated in **Figure 10**. This depiction assumes that the kinetics of the redox couple are fast, but it is well known that many environmental systems are far from thermodynamic equilibrium (Schüring et al. 2000).

Electric double layer

The distribution of aqueous ions near the surface of a mineral in water is affected by the presence of an electrostatic potential at this interface. Such surface potentials can be created by equalization of the Fermi levels in the solid and the electrolyte (as described above) and by the chemisorption of charged solution species to the mineral surface. For a given mineral surface, strongly interacting charged species are called potential determining ions (PDI) (Lyklema, 2001). For example, H^+ and OH^- are PDI for metal oxides, while HS^- can be a PDI for sulfide minerals (Bebie et al. 1998). The pH driven shifts in oxide band energies are quantitatively described by the Nernstian relation that predicts a shift of 0.059 V/pH at 25 °C and 1 atmosphere pressure. However, there are apparently no experimental tests of this relation for nanoscale particles. Similarly, although nanoparticles (and colloids in general) act as ready sorbents for inorganic and organic ions and molecules, the effects of different sorbates on band positions are generally not known. The adsorption of redox active solution species seldom affects the energy band positions.

REDOX BEHAVIOR OF NANOPARTICLES

Having completed a brief review of the factors that affect the energies of electronic bands in solids, we are now able to apply this knowledge to the

(photo)chemical reactions of nanoparticles. The fundamental reactions in which nanoparticles can participate are depicted in **Figure 11**.

Size effects on nanoparticle redox behavior

The modification of the absolute valence and conduction-band energy levels is a predominant effect on redox behavior when it occurs. As discussed above, doping of a semiconductor, sorption of potential determining ions, and finite particle size may all contribute to such effects.

Examples of size effects on redox potential

As shown by Brus (1984), and reproduced in **Figure 8a**, finite size effects can have a large impact on the redox potentials of semiconductors (see also Franschetti et al. 2000). However, the extent to which valence electrons are delocalized and hence susceptible to finite size effects is unclear for several environmentally relevant materials. For example, sphalerite (ZnS) and pyrite (FeS₂) are, respectively, direct and indirect delocalized electron semiconductors in which quantum confinement effects will occur. **Figure 8b** plots the size-dependent shifts in the VB and CB levels for these materials predicted by the EMA.

It is presently difficult to anticipate quantum confinement effects in environmental iron and manganese compounds for which electron and hole effective masses have not been tabulated. Nevertheless, a recent x-ray spectroscopic study identified an increase in the band gap of hematite nanorods ~ 4 nm in diameter by approximately 0.3 eV (Guo 2005). UV-vis spectroscopy of encapsulated iron oxide nanoparticles also indicated size-dependent band-gap opening (Iwamoto et al. 2000). In common with most iron (III) and manganese (IV) (oxyhydr)oxide minerals, the conduction and upper valence bands have the character of cation *d*-states, while the lower valence band is principally composed of oxygen *p*-like orbitals, although covalency in the metal-oxygen bond causes mixing in the valence band states (Cox 1992, Sherman 1984, Sherman 1985, Sherman 2005). In **Figure 8b**, we predict the size dependence of the hematite band gap using an estimate for the effective masses of charge carriers (assuming

$m_e^* = m_h^*$) consistent with the observations of Guo (2005). Band-gap opening, as depicted in **Figure 8**, will significantly affect mineral reactivity (Rodriguez et al. 1998). The predictions of **Figure 8** require further experimental testing, particularly the use of combined x-ray absorption and emission spectroscopic measurements of nanoparticle band gaps (Lüning et al. 1999, Sherman 2005), and more sophisticated theoretical treatments (O'Connor & Sposito 2005).

A complementary approach for understanding the electronic properties of mineral nanoparticles will be studies of the kinetics of surface reactions. Kinetics studies have been used to determine the relative reactivities of different iron minerals to surface redox or complexation reactions (Poulton et al. 2004, Elsner et al. 2004, Hering & Stumm, 1990, Peak 2005). Such studies provide a method for determining size-dependent changes in surface reactivity (see below; Madden & Hochella 2005).

The roles of surface states

Atoms at the surface of a material are not generally able to attain the same coordination environment that is present within the interior. Thus, atomic sites at a surface may exhibit modified local electronic structure that in some cases can introduce energy levels within the band gap of a semiconductor or insulator (Morrison 1980). Surface states can therefore have the same effect as interior impurity atoms, either facilitating the creation of mobile electron or hole charge carriers or acting as traps for them. For example, underbonded surface anions can donate electrons into the CB of the mineral (cf. **Figure 16**). Surface states can also mediate the transfer of charge between an adsorbate and states within a mineral or between two aqueous or adsorbed reagents. In addition, the trapping of electrons at surface states can affect the lifetime of photoexcited electrons and holes, and can determine the rate of electron transfer between neighboring particles (see below).

The above phenomena occur at the surfaces of both bulk minerals and nanoparticles. The surfaces of nanoparticles are structurally more diverse, and molecular simulations indicate that inhomogeneous charge distributions can occur at nanoparticle surface and edge sites, modifying the surface Lewis acid or base characteristics relative to large particles (Lucas et al. 2001, Noguera et al. 2002, Rustad & Felmy, 2005).

Scanning tunneling spectroscopy (Preisinger et al. 2005) and optical luminescence spectroscopy (Chen et al. 1997) are approaches for detecting surface states that lie in the electronic band gap. However, environmental nanoparticles and their synthetic analogs are poorly studied.

Undercoordinated surface sites tend to be more reactive and hence are frequently the sites at which molecules bind to nanoparticle surfaces. In place of the initial surface states, new surface-ligand molecular orbitals are formed, with discrete energy levels that may no longer reside within the band gap. While ligand binding has been extensively studied for the removal of mid-gap states in engineered nanoparticles (e.g., Green & O'Brien, 1999), ligand binding can also create (photo)redox active mid-gap energy states (e.g., Rajh et al. 2002)

Examples of nanoparticle redox behavior

Nanoparticles as molecular-like redox active solution species

Nanoparticles can accept or donate electronic charge, and in this sense can be considered redox active species. **Figure 12** shows that CdS nanoparticles can diffuse to, and react with an electrode in an electrochemical cell in a manner similar to an aqueous ion (Kukur et al. 2003). The potential at which the nanoparticles can be reduced (i.e., charged by a single electron) varies with particle size in agreement with confinement effects. However, even for nonaggregated nanoparticles, diffusion rates are considerably slower than dissolved ions or molecules (Scholz & Meyer, 1998). The Brownian diffusion rate for nanoparticle transport is given by the Stokes-Einstein equation:

$$D = \frac{k_B T}{6\pi\eta r}, \quad (13)$$

where η is the solution viscosity, and r is the particle radius. The implication of the results of **Figure 12** is that nanoparticles are available to participate in molecular redox reactions with aqueous ions and biomolecules. Below, we discuss the important issue of the stability of individual nanoparticles during (photo)redox reactions.

The example above is one of a number of experimental investigations of the charging of nanoparticles that was conducted at electrochemical electrode (Haram et al. 2001, Kukur et al. 2003, McKenzie & Marken, 2001). In nature, redox active solution species can inject electrons into the conduction band of a mineral, provided that the redox potential of the aqueous redox reaction is more negative than the position of the CB minimum. For example, Cd(II) and Co(II) can be oxidized on the surface of ZnO and manganese (IV) oxides, respectively (Murray & Dillard 1979, Manceau et al. 1997). In the opposite direction, electrons may transfer from the mineral VB to a strongly oxidizing organic species such as ascorbic acid, which can cause the direct oxidation of manganese oxide minerals (Stone & Morgan 1984, Stumm & Morgan 1996).

A negatively charged nanoparticle is free to act as a reductant with a suitable acceptor species. If further charge transfer to the nanoparticle carries an energy penalty (see below), additional reactions with donor species are not favored the excess charge has been lost. An important question is whether oxidant and reductant must be simultaneously surface bound, or whether charged nanoparticles can be formed that are sufficiently stable in solution to act as reactive intermediates. The direct reaction scheme can be written



where $\lambda > D$ represents donor species D adsorbed onto a nanoparticle. Alternatively:



For electron transfer reactions, the donor (or acceptor) species and the nanoparticle must (1) have a redox potential that coincides with electron energy bands in the minerals, and (2) attain sufficient wavefunction overlap with these bands (Huber et al. 2000). Many single-electron transfer reactions can occur via electron tunneling to or from species bound to the surface by outer-shell adsorption. However, ligand-particle electron transfer rates are greatly enhanced by surface complexation (Moser et al. 1991); and

certain charge transfer reactions, particularly involving Fe *d*-electron states, require inner-sphere surface coordination to proceed at all (e.g., Ennaoui & Tributsch, 1986).

The possibility of multiple oxidation states of nanoparticles

The energy required to singly charge a solvated nanoparticle (**Figure 11a**) is sensitive to both the nanoparticle size and the dielectric constant of the solvent (Franceschetti et al. 2000). The addition of subsequent electrons to an already charged nanoparticle is possible, but additional energy may be required to compensate for Coulomb repulsion if there is electronic overlap between CB electrons (Brus, 1984). In this case, nanoparticles can behave more like atoms with variable redox states (Banin et al. 1999), than bulk minerals within which excess charges may diffuse apart.

Atomic-like redox behavior would lead to a quenching of bioreductive processes involving nanoparticles, because the successive charging energies would eventually exceed the reducing power of extracellular electron shuttle molecules. However, this is not observed for the biological reduction of ferric iron minerals, since phases with higher surface areas (i.e., smaller particle size) are more completely reduced (Roden & Zachara 1996, Hansel et al. 2004). For minerals composed of atoms susceptible to valence changes, mineral dissolution is an effective pathway for shedding excess charge. Furthermore, in the small polaron model of charge transport in localized carrier materials, an additional electron at an iron site is spatially localized within a radius less than the near-neighbor bond length (Cox 1992). This implies that interactions between multiple ferrous iron sites will be weak, and that the energy required to add an electron to a ferric iron nanoparticle will not depend on the number of excess electrons already hosted, in contrast to the behavior of delocalized band semiconductors.

Reductive transformation of halogenated organic contaminants

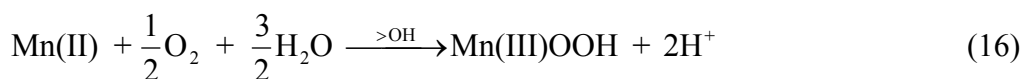
Many relevant investigations have been motivated by the desire to identify natural pathways for immobilizing or transforming organic or inorganic contaminants. For example, Fe(II) adsorbed to the surface of ferric iron and non-iron-containing minerals can be a powerful reductant, one that can transform hazardous chlorinated hydrocarbons such as carbon tetrachloride (CT) (Pecher et al. 2002, Elsner et al. 2004) and chromate

(Wielinga et al. 2001). Mineral surfaces that stabilize the Fe(III) product of the oxidation of surface-bound Fe(II) can lower the Fe(II)-Fe(III) redox potential (Stumm & Morgan 1996, Amonette et al. 2000, Pecher et al. 2002). Structural Fe(II) in mixed-valence iron oxide compounds such as magnetite, particularly biogenic magnetite nanoparticles, can also transform CT.

As shown by **Figure 13**, numerous electron shuttle molecules used by anaerobic DFeRB also possess reduction potentials that can degrade CT, and co-metabolic pathways do contribute to the natural attenuation of this compound. However, in laboratory studies, biogenic magnetite is approximately two orders of magnitude more effective than biomolecular pathways (McCormick et al. 2002, McCormick & Adriaens, 2004). Nanoscale magnetite also reduces U(VI) to U(IV) under anaerobic conditions (following surface adsorption) much more rapidly than occurs in solution under reducing conditions (Missana et al. 2003).

Surface-promoted redox reactions

Bulk mineral surfaces can mediate charge transfer between solution species that otherwise interact too weakly for effective redox pathways. For example, sulfide minerals—including pyrite, galena, and several doped sphalerite minerals—catalyze the oxidation of thiosulfate to tetrathionate by dissolved molecular oxygen (Xu & Schoonen 1995). A significant nanosize effect was recently observed for hematite-promoted Mn oxidation (Madden & Hochella, 2005). While the oxidation of aqueous Mn(II) by oxygen is very slow at pH < ~8.5, it may be promoted following adsorption to mineral surfaces. Surface hydroxyl groups (denoted >OH) mediate electron transfer from molecular oxygen to adsorbed manganese, facilitating the reaction:



As shown in **Figure 14**, the kinetics of this reaction, normalized to surface area, exhibit an increase of more than one order of magnitude for 7 nm diameter hematite nanoparticles compared with 37 nm particles. Madden & Hochella (2005) discuss the

possible origins of this striking enhancement of reactivity. Hematite energy bands do not play a direct role in this process; hence, electronic confinement effects are unlikely to be responsible. Possible explanations of the rate enhancement may be understood from Marcus's original description of the rate of electron transfer (Marcus 1993). By setting $\Delta G^* = (\Delta G^o + \lambda)^2 / 4\lambda$ in **Eqn 5**,

$$k_{et} = \kappa \nu \exp\left(-\frac{(\Delta G^o + \lambda)^2}{4\lambda k_B T}\right) \quad (17)$$

where ΔG^o is the standard free energy of the reaction (positive or negative) and λ is the reorganization energy (always positive). Size-dependent changes in either ΔG^o or λ are plausible and would modify the reaction kinetics, provided that electron transfer is the rate-limiting step.

For example, it is likely that the redox potential of Mn(II) adsorbed to the smaller particles is shifted because of a size-dependent modification in the Lewis base character of oxygen atoms on the surface of the hematite to which Mn adsorbs (Noguera et al. 2002, Lewis et al. 2001). If this drives the ΔG^o of **reaction 16** more negative, Mn oxidation would not only be more favorable, but k_{et} would increase.

Alternatively, small particles may exhibit a higher density of surface sites at which the coordination geometry of adsorbed ions is distorted from the perfectly octahedral configuration preferred by Mn(II). However, Mn(III) complexes tend to prefer a distorted octahedral coordination. Therefore, if the smaller nanoparticles possess greater surface disorder, less structural reorganization may be necessary for the reaction to proceed. This effect would reduce λ , thereby increasing k_{et} .

The results of Madden and Hochella (2005) demonstrate that the redistribution of both charge and atoms at the surfaces of nanoparticles may strongly influence their reactivity. EXAFS investigations into changes in the coordination environment of Mn(II) bound to hematite nanoparticles in the absence of oxygen may help evaluate these two models.

PHOTOCHEMISTRY

A photon of energy greater than the band gap can excite a valence electron to the CB, which leaves a vacant orbital (hole) in the VB. The excited electron (hole) has the ability to reduce (oxidize) chemical species at the surface of the nanoparticle. As with redox chemistry, the ability to do this depends on the absolute electron or hole energy, and hence can be affected by particle size (and pH), as described above.

Size effects on nanoparticle photochemistry

Kinetics of recombination and reaction

Following photoexcitation of a nanoparticle, several processes can occur that facilitate or prevent reaction, and these processes may exhibit distinct small-size effects (Gratzel & Frank, 1982, Gerischer 1993). Diffusion of an excited electron or hole to the surface and transfer to surface species competes with the recombination of the electron-hole pair and trapping at surface states (Zhang 2000). The transit time to the surface varies as the square of the particle radius, and is generally less than 1 ps for few-nm diameter particles (Gratzel & Frank, 1982, Huber et al. 2000). The recombination time is principally material dependent, with a weak size dependence caused by enhanced electron-hole overlap. Since the recombination time is generally in the range 0.1 – 1 ns, excited electrons have a far greater probability of reaching the surface of nanoparticles than larger colloidal particles, such as >100 nm diameter iron oxide colloids, in which most electron-hole pairs recombine before reaching the surface (Leland & Bard, 1987).

Nanoparticle surface states can act as traps for excited electrons with lifetimes that may vary by many orders of magnitude for different nanoparticles. If a photoexcited electron or hole is *scavenged* by a solution or surface species, recombination within the nanoparticle is no longer possible, and the nanoparticle can remain excited for a considerable time (e.g., minutes) (Leland & Bard, 1987).

Because both a hole and electron are created following light absorption, both cathodic (i.e., reduction) and anodic (i.e., oxidation) reactions are possible at a nanoparticle surface and may proceed in very close proximity. The kinetics of these

reactions are seldom equivalent, providing an opportunity for reaction intermediates to interact. Several studies have concluded that competition between the above processes, plus variation in surface area:volume ratio, leads to an optimum particle size for the maximum efficiency of a given photoreaction that is frequently in the 5–20 nm diameter range (Wang et al. 1997, Almquist & Biswas 2002).

Reactions requiring multiphoton absorption

The probability of a photoexcited nanoparticle absorbing a second photon declines with particle size for statistical reasons (Wang et al. 2003), and hence reactions requiring rapid multielectron transfer are highly unlikely for nanoscale particles under environmentally relevant illumination conditions. For example, the products of the photooxidation of ethanol are different for micron-sized versus nanometer-sized ZnS colloids (Müller et al. 1997). Under constant illumination, transfer of two photoexcited holes to adsorbed ethanol can occur readily within 200 ns on the surface of the larger particles. By contrast, the mean time to create two holes in a nanoparticle reaches several seconds, permitting partially oxidized ethanol radicals to diffuse into solution and form more complex organic species.

Shifts in electronic band energy positions

The effect of particle size on the photoredox activity of nanoparticles can be illustrated through analogy, with the effect of pH on the photoreduction of methylviologen ions (MV^{2+}) at the surface of colloidal TiO_2 particles (Duongdong et al. 1982). The half-reaction, $MV^+ \leftrightarrow MV^{2+} + e^-$, has the redox potential $E_o = -440$ mV versus NHE that is independent of pH. By contrast, the electrochemical potential of the TiO_2 CB varies with pH as

$$E_{CB}(TiO_2) = E_{CB}(TiO_2, pH\ 0) - 0.059(pH)\ V\ (vs.\ NHE) \quad (18)$$

As shown in **Figure 15**, photoexcited electrons in the CB are sufficiently reducing only above pH around 4-5. Photoreduction of MV^{2+} is thermodynamically forbidden below this pH threshold. As shown below, for materials that exhibit size-dependent shifts in CB

position, thresholds in particle size can exist below which photoredox reactions are enabled.

For completeness, should be recalled that changes in pH can strongly affect the affinity of ionic sorbates to surface binding sites, particularly around the point of zero surface charge (pH_{zpc}) for a material (Kormann et al. 1991). Such effects can complement or compete with shifts of the nominal redox potentials of CB electrons and VB holes.

Nanoparticle interactions with biomolecules

It is clear from the study of environmental colloids that mineral surfaces can exhibit high affinities for organic molecules (Yariv & Cross, 1979, Amal et al. 1992, Tiller & O'Melia 1993), and many groups have demonstrated effective surface binding of molecules to sulfide and oxide nanoparticles via assorted terminal functional groups. In particular, biomolecules such as amino acids, phospholipids, siderophores, and even DNA have been shown to stabilize sites on nanoparticle surfaces (Konovalova et al. 1999, Jones et al. 2000, Torres-Martínez et al. 2001, Dwarakanath et al. 2004). Recent studies have addressed the detailed electronic structure associated with functional groups on bacterial surfaces, including the position of the Fermi level (Vyalikh et al. 2004, Ireta et al. 1998), which will permit quantitative treatments of nanoparticle-microorganism interactions. As discussed above, strong chemical interactions can create new electronic states in the mineral, modifying (photo)redox reactivity. The coupled redox reactions of iron and manganese oxides and biomolecules play a vital role in the transformation of organic matter and the production of humic materials.

Interestingly, while hydrated biofilms may considerably coat the surfaces of minerals, they appear not to seriously hinder the surface adsorption and reaction of either small molecules or metal cations (Templeton et al. 2003, Toner & Sposito, 2005), although certain aqueous ions may partition between mineral surface sites and organic functional groups depending upon pH (Warren & Haack 2001).

Roles of adsorbed surface species in redox and photochemistry

The complexation of surface atoms of a nanoparticle by adsorbed molecules can introduce additional electronic states within the semiconducting band gap (see **Figs 11f and Fig. 17**), a phenomenon termed *sensitization*. Sorbates can significantly increase the rate of photochemical reactions, because the photon energy threshold for creating an excited electron or hole in electronic bands of the nanoparticle can be greatly reduced (Konovalova et al. 1999, Rajh et al. 2002). Charge injection from the adsorbate to the nanoparticle is generally extremely fast (< 0.1 ps), while electron transfer back to the adsorbate, which would permit electron-hole recombination, may take milli- or even microseconds (Moser et al. 1991, Huber et al. 2000).

A series of important experiments by the group of Rajh have shown that organic molecules possessing enediol groups ($-\text{CHOH}=\text{COH}-$) bind to and hybridize with several metal oxide nanoparticles (**Figure 16**, Rajh et al. 2002). This process is particularly efficient because undercoordinated cations on the surfaces of Fe_2O_3 and TiO_2 nanoparticles sit within considerably distorted sites. Ligand binding restores local octahedral symmetry and is energetically very favorable. Furthermore, Rajh et al. (2004) showed that single-stranded DNA binds to the surface of TiO_2 nanoparticles and retains the ability to hybridize with complementary DNA. Following direct photoexcitation of the nanoparticle, charge transfer occurs readily onto double stranded DNA, but not single-stranded DNA.

Examples of nanoparticle photochemistry

Photofixation of CO_2

There is a considerable technological effort behind using colloidal particles for harvesting solar energy, not only for electrical energy production, but also for performing benign photochemistry, such as the splitting of water (Bard & Fox 1995) or the photocatalytic degradation of organic environmental pollutants (Hoffmann 1995). Following Inoue et al. (1995), the photoreductive “fixation” of atmospheric CO_2 has been studied by many groups. In most engineered systems, this pathway has always been rather inefficient, although several groups have claimed improvements using

chalcogenide nanoparticles including ZnS and CdS (Fujiwara et al. 1997, Fujiwara et al. 1998). The reaction begins with the step:



where $> \text{CO}_2^{\bullet -}$ indicates a surface-bound CO_2 radical. $\text{CO}_2^{\bullet -}$ is extremely reactive and, following desorption into water at pH 7, produces formic acid (HCOOH), CO , and H_2 (Fujita & DuBois 2003).

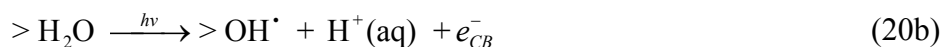
First-principles calculations have shown that two effects (one structural, one purely electronic) can together explain the experimental observation that nanoparticles of CdSe are capable of photofixation of CO_2 (Wang et al. 2002), a process not observed for bulk CdSe (Nedeljkovic et al. 1986). As shown in **Figure 17**, CO_2 molecules may chemisorb at Se vacancies on a nanocrystal surface. Because the CB lies at higher energy in the nanocrystals than in the bulk, photon absorption creates an excited electron with a redox potential capable of reducing the sorbed molecule to produce a reactive charged radical, with a low energy barrier to desorption. Subsequent reactions can create small organic molecules such as formic acid.

There is no evidence that nanoparticle production fulfills a biological role of encouraging CO_2 fixation. Nevertheless, the above mechanism is one way that nanoscale minerals affect organic carbon transformations. Moreover, it illustrates the capacity for nanoscale minerals to generate reactive radicals.

Photogeneration of reactive oxygen species

Photogenerated radicals derived from water or oxygen are commonly found to be reactive intermediates during heterogeneous photochemical reactions (Gerischer 1993, Hoffmann et al. 1995, Riegel and Bolton 1995, Hall 2000, Torres-Martínez et al. 2001, Garrett et al. 2005). The principal reactive species are formed by the capture of a photoexcited electron or hole by surface-adsorbed molecular oxygen or water, respectively:





Hydroxyl radicals typically remain surface bound and can be considered as holes trapped at surface states (Lawless et al. 1991), while the superoxide anion, $\text{O}_2^{\bullet-}$, may diffuse into solution. Further reduction of $\text{O}_2^{\bullet-}$ can generate hydrogen peroxide, H_2O_2 , but H_2O_2 is not evolved under anaerobic conditions.

All of the reactive oxygen species can cause cellular damage (Hall 2000), and interactions between nanoparticles and biomolecules can increase the type and number of reactive oxygen species produced photochemically. For example, the yield of $\text{O}_2^{\bullet-}$ during photoexcitation of TiO_2 is greatly enhanced by the presence of low-concentration carotenoid sensitizers (Konovalova et al. 2004). Furthermore, extracellular electron shuttles such as quinones (Newman & Kolter 2000, Nevin & Lovely 2000) can act as diffusible secondary reactive intermediates that propagate cell toxicity (Bolton et al. 2000). However, certain strongly bound surface ligands such as halogenated acetic acids may be oxidized directly without a role for reactive intermediates (Pehkonen et al. 1995). The photoactivity of specific minerals cannot always be predicted from thermodynamic considerations and many environmental minerals are not well studied. The combination of sunlight and dissolved oxygen is required for significant photogeneration of cytotoxic radicals, limiting the impact of these processes to near-surface environments.

The stability of nanoparticles during redox chemistry and photochemistry

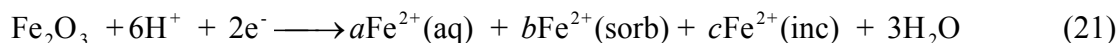
Stability during redox reactions

An excess or deficiency of charge in a nanoparticle may be delocalized within electronic bands or localized at atomic sites, depending upon the mobility of charge carriers within the mineral. Redox active atoms within a nanoparticle may capture the electron or hole through a valence state change, which can lead to nanoparticle dissolution. Dissolution of insoluble ferric iron and manganese oxide minerals may occur following charge injection from a solution donor (**Figure 11a**) (Hering & Stumm, 1990), which can include biological electron-transfer molecules (Newman & Kolter, 2000, Cheah et al. 2003) or molecular “nanowires” (Reguera et al. 2005), sufficiently reducing

inorganic (Missana et al. 2003) or organic (McCormick et al. 2002) species, or photoexcited ligands (Voelker et al. 1997).

Reductive dissolution of hematite

Direct electrochemical measurements of Fe₂O₃ nanoparticles drive dissolution, once the electrode potential is sufficiently negative to reduce the iron oxide particles (McKenzie & Marken, 2001). The chemical reductive dissolution of hematite can be driven by numerous reductants (Stumm & Morgan 1996), including dissolved sulfide (Dos Santos Afonso et al. 1992, Poulton et al. 2004). When the reductive dissolution of ferric iron oxides was quantified (using a radiologically generated reductant), the amount of dissolved Fe(II) plus adsorbed Fe(II) could not account for all the reductant consumed (Mulvaney et al. 1988). The reductive dissolution of hematite can be written:



where the prefactor a is the fraction of reduced iron liberated into solution, b is the fraction adsorbed at the surface, and c is the fraction of electrons incorporated in the interior of the colloidal particles ($a + b + c = 2$). The prefactors exhibit a strong pH dependence as expected, and vary with colloidal particle size. Around neutral pH, $c \approx 0.25$ for 5 nm diameter particles, but $c \approx 0.7$ for micron-sized colloids. Thus, some ferrous iron sites are indefinitely stabilized within ferric iron minerals. The partially reduced minerals are likely an intermediate step in the solid-state transformation to magnetite, perhaps with a disordered structure analogous to the that found as a thin layer upon hematite colloids (**Figure 2**; Hansel et al. 2004). The partially transformed nanoparticles are reductants themselves, with an activity that depends both on the effective redox potential of structurally incorporated Fe(II) and its mobility, and partitioning between the surface and interior (Williams & Scherer, 2004). As expected, higher-surface-area particles are more effectively dissolved, but even the smallest nanoparticles retain a number of ferric sites.

Stability during photoredox reactions

Many semiconductors that are stable against reductive surface processes can be subject to *photocorrosion* (Gerischer 1980, Memming 2001). If a nanoparticle participates in the light-stimulated reduction of an acceptor molecule, a hole remains in the VB (**Figure 11e or f**). From a molecular perspective, a hole is a partially broken bond (albeit a potentially mobile one). Similarly, a photo-oxidation event (**Figure 11d**) entails the production of excited electrons that may drive a local valence state change at Fe(III) and Mn(IV) sites and detachment of the atom (i.e., dissolution).

Photoreductive dissolution of hematite

Sherman (2005) combines oxygen x-ray absorption and emission spectroscopy to determine the conduction and valence-band energy positions of bulk iron and manganese oxides and oxyhydroxides. The position of the hematite CB relative to the redox potential for hematite dissolution determines whether photoexcitation of the mineral (**Figure 11c**) can lead to dissolution. Since at pH 2, $E_o = 0.655$ V for $\text{Fe}^{2+}/\alpha\text{-Fe}_2\text{O}_3$, assuming an aqueous concentration of ferrous iron to be $[\text{Fe}^{2+}] = 10$ nM, and $E_{CB}^{\text{hematite}} = 0.3$ eV, direct photodissolution will occur at pH 2, but not at circumneutral pH.

At pH 8.3, the bulk hematite CB is predicted to lie ~ 0.4 eV below the $\text{Fe}^{2+}/\alpha\text{-Fe}_2\text{O}_3$ couple on the AVS scale (Sherman 2005). However, as indicated in **Figure 8b**, hematite nanoparticles with a diameter of ~ 2 nm are predicted to possess sufficiently reducing CB electrons for photodissolution to proceed at pH 8. Because of the increase in the band gap, higher energy photons would be required to drive photodissolution of the smaller particles.

The presence of additional solution species can also favor the photoreduction of hematite, either by sensitizing the mineral surface (Pehkonen et al. 1995) or by complexing soluble Fe(II) so that the electrochemical potential for iron reduction is made more positive (Kraemer 2004) and lies beneath the CB.

Ligand promoted photoreductive dissolution of manganese oxide

Manganese oxides in the presence of dissolved organic matter are sensitive to photoreduction (Sunda et al. 1983, Scott et al. 2002, Haack & Warren 2003). Following light absorption by an adsorbed ligand (e.g., humic and fulvic acids; ascorbic acid), fast

injection of an electron into the mineral VB (**Figure 11f**) can drive reduction of Mn(IV) to Mn(II), which is subsequently soluble. Since this is a two-electron process, the dissolution rate will depend upon the mobility of electrons in the mineral and is likely to exhibit a significant dependence on particle size. Manganese reduction performs an important role in the redox cycling of Mn, and can impact the bioavailability of nutrient and contaminant adsorbates by releasing them into solution (Crerar et al. 1976). Daily cycles in the quantity of oxidized Mn in a biofilm of Mn oxidizers are consistent with sunlight-driven photodissolution (Bourg & Bertin, 1996, Haack & Warren, 2003).

Photodecomposition of sulfides

Metal sulfide particles are susceptible to photodecomposition in the presence of oxygen (which acts as an electron acceptor), producing soluble metal and sulfate ions. Although stability is greater in anaerobic environments, other solution species, such as sulfite ions, can act as electron donors. For example:



While the thermodynamics of photodecomposition reactions are known in many cases (Gerischer 1980, Memming 2001), it can be hard to predict particle stability for arbitrary solution chemistry (Kormann et al. 1989).

Nanoparticle interactions with microorganisms

The possibility of nanoparticle uptake

When biomineralization serves no known structural, navigational, or nutrient storage function, microorganisms almost universally attempt to restrict the precipitation of solids to the extracellular regions. The cell walls of both Gram positive and Gram negative bacteria (both negatively charged at circumneutral pH) present a considerable barrier to nanoparticle transport (Beveridge 1981, Fortin et al. 1997). However, as illustrated by **Figure 18**, nanoparticle precipitation frequently occurs to high densities in the periplasm. Presently, most studies on nanoparticle uptake are limited to mammalian

cell lines, which in contrast to prokaryotic cells are able to acquire nanoparticles by endocytosis (Parak et al. 2002, Alivisatos et al. 2005). Mechanisms of prokaryotic nanoparticle uptake are (1) nonspecific diffusion through membranes, (2) nonspecific membrane damage-mediated uptake and (3) specific uptake following membrane binding. Metal chalcogenide nanoparticles (such as CdSe) can be internalized within both Gram positive and Gram negative bacterial species via a pyrene-dependent mechanism provided that the surface is labeled with adenine or (AMP) and that the diameter of the coated nanoparticle is less than 5 nm (Kloepfer et al. 2005). As particle uptake exhibits both a dependence on surface label and light exposure, it is likely that a combination of mechanisms 2 and 3 above is responsible for the nanoparticle uptake.

Nanoparticle uptake may facilitate gene transfer. It has been shown that the association of DNA with nanoscale precipitates of calcium phosphate minerals greatly enhanced the efficiency of gene transfer into human cell cultures over what was observed for aqueous DNA in the absence of minerals (Shen et al. 2004). It was unclear whether nanoparticles acted as a vector that carried DNA into the cell, or whether the DNA was released from the nanocomposite before uptake. Nevertheless, such studies indicate that extra-cellular biomineral-associated DNA has the potential for colloid-facilitated transport within the environment, while retaining the capacity for subsequent gene transfer.

Nanoparticle aggregation and its consequences

The electron micrographs of **Figure 1** suggest that biogenic nanoparticles are seldom present as individual particles, but exhibit a marked tendency for aggregation and deposition onto cell bodies. These processes are governed by particle-particle and particle-cell interaction forces that include electrostatic Coulombic forces (resulting from net charge on the nanoparticle surfaces) and short-range dispersion or van der Waals forces. The classical description of colloid stability—DVLO theory—has been intensely investigated for microscopic colloids (Verwey & Overbeek, 1948, Lyklema 2001), although quantitative discrepancies remain, particularly at high ionic strength (Israelachvili 1992, Boström et al. 2001). In particular, suspensions of colloids separated

by net repulsive forces are generally found to be less stable against aggregation than predicted by DVLO theory. Furthermore, the validity of this description has not been established for nanoscale particles, for which a continuum description of the electrical double layer may not be appropriate. Nanoparticle transport and settling behavior is highly affected by the colloid properties of the individual particles, but remains a difficult process to quantify (Elimelich et al. 1995, Tiller & O'Melia 1993). Nanoparticle aggregation processes are beyond the scope of this chapter, so we simply state that numerous experimental studies have shown that mineral particles can be unstable against aggregation at circumneutral pH, and that the resulting aggregates commonly possess a complex interior porosity with the characteristics of geometric fractals (Meakin 1988, Dickinson 1989, Amal et al. 1990, Mylon et al 2004).

Charge transport in aggregated nanoparticles

Aggregates of semiconductor nanoparticles have been shown to be surprisingly efficient at transporting electrons that have been excited to the conduction band (**Figure 11g**) (Wang et al. 2003). This process is initiated particularly effectively by photoexcitation of surface sensitizer molecules (**Figure 11f**, where A = second nanoparticle). When the rate of back transfer is slow, the lifetime of the excited electron is sufficiently long to permit its transport to a CB of a neighboring nanoparticle. Particle-particle charge transfer separates the original electron and hole, which then persist until consumed in a chemical step, such as redox reaction or radical formation.

Charge transfer between two nanoparticles occurs via a mechanism analogous to electron hopping between localized sites in a crystal. The analogy is quite good, because electronic states on the nanoparticle surfaces trap the electron between particle-particle transfer steps. Typical shallow electron traps on TiO₂ surfaces are 25–50 meV below the CB (Hoffmann et al. 1995), so thermally activated transport is possible at room temperature ($k_B T \approx 25$ meV at 25 °C). However, while a single activation energy barrier typically limits hopping between atomic sites in a crystal, there is generally a broad range of surface states on nanoparticles and hence a distribution of activation energies (Nelson 1999).

There are now numerous measurements of the conductivity of nanoparticle aggregates. Theoretical descriptions of conductivity are based on percolation (for fractal aggregates, Avnir, 1989) or diffusion models (for nonfractal compact aggregates, Nelson 1999). These approaches are not too sensitive to the details of the particle-particle transfer mechanism and can provide good agreement with experiment.

The factors that determine whether electron transport occurs predominantly via nanoparticle surface or interior states remain unclear. This issue has been addressed with temperature-dependent conductivity measurements across arrays of magnetite nanoparticles. In one study on 5.5 nm diameter nanoparticles, a conductivity drop was seen below metal-insulator transition temperature, a clear sign of bulk-mineral-like conductivity (Poddar et al. 2002). In a second independent study of 14 nm particles, no temperature-dependent effect was observed, suggesting that surface-mediated conduction dominated (Redl et al. 2004).

Significantly, many investigations of the conductivity through aggregated nanoparticles have been performed on dried layers of deposited particles. However, surface hydration can increase electron transport by orders of magnitude, even when direct conductivity through the liquid is not possible. As shown by Brus (1996), in a series of calculations for porous Si, electrons can couple to the dynamics of solvent molecules, which provides an activated intermediate state for transfer between particles. Charge transfer is considerably more favorable in a polar solvent than in air or vacuum because as a consequence of the solvent, the donor and acceptor energy levels do not have to be closely spaced.

Exciton transport in aggregated nanoparticles

Long-range energy transfer (also known as Förster energy transfer) is an electrostatically mediated transfer of energy between two molecules or nanoparticles that have resonant excitation energies (**Figure 11h**). Significant energy transfer is only possible if the acceptor has a fast-energy-loss pathway to trap the excitation that otherwise can transfer back to the donor. No activation energy is required, but diffusion of excitations is the dominant process for separations less than ~ 5 Å. Long-range energy has been demonstrated among aggregated nanoparticles (Kagan et al. 1996) and between

nanoparticles and a surface (Achermann, 2004), but it is presently not known to be significant in biogenic nanoparticle aggregates.

CONCLUSIONS

Nanoparticles are integral constituents of water bodies, sediments, and soils, and many microorganisms that rely on an inorganic component to their metabolism inevitably interact with nanoscale minerals. Individual nanoparticles have the capacity to act as mobile redox active species that participate in molecular-style redox reactions. The redox potentials of valence and conduction band electrons, and the kinetics of charge transport and particle diffusion can exhibit a strong dependence on particle size. However, the susceptibility of minerals to dissolution upon valence change means that, in contrast to true molecular reagents, charged or photoexcited nanoparticles generally have mechanisms for transformation and energy loss that are not observed in molecular species. Biogenic nanoparticles form extended aggregates with complex structural, surface chemical and charge transport properties. The surfaces of nanoparticles and their aggregates generally exhibit strong affinity for aqueous nutrients, contaminants and organic biomolecules, including DNA, and can promote (bio)geochemical redox reactions, in some cases at significantly greater rates than observed at the surfaces of bulk minerals.

Acknowledgments

We thank Pupa de Stasio, Glenn Waychunas, Ken Nealson and Dan Hawkes for reviewing the manuscript, and Clara Chan, John Moreau, Yohey Suzuki, and Ken Williams for generously permitting reproduction of electron micrographs.

References

Abdelouas A, Lutze W, Gong WL, Nuttall EH, Strietelmeier BA, Travis BJ (2000) Biological reduction of uranium in groundwater and subsurface soil. *Sci Tot Environ* 250: 21-35.

Achermann M, Petruska MA, Kos S, Smith DL, Koleske DD, Klimov VI (2004) Energy-transfer pumping of semiconductor nanocrystals using an epitaxial quantum well. *Nature* 429: 642-646.

Adams MA, et al. (2003) Charge transfer on the nanoscale: Current status. *J Phys Chem B* 107: 6668-6697.

Alivisatos AP (1996) Perspectives on the physical chemistry of semiconductor nanocrystals *J Phys Chem* 100: 13226-13239

Alivisatos AP, Gu W, Larabell C (2005) Quantum dots as cellular probes. *Annu Rev Biomed Eng* 7:8.1 – 8.16

Almquist CB, Biswas P (2002) Role of the synthesis method and particle size of nanostructured TiO₂ on its photoactivity. *J Catalysis* 212: 145-156

Amal R, Raper JA, Waite TD (1992) Effect of fulvic acid adsorption on the aggregation kinetics and structure of hematite particles. *J Colloid Interf Sci* 151: 244-257.

Amonette JE, Workman DJ, Kennedy DW, Fruchter JS, Gorby YA (2000) Dechlorination of carbon tetrachloride by Fe(II) associated with goethite. *Environ Sci Technol* 34:4606-4613.

Ashcroft NW, Mermin ND (1976) *Solid State Physics*. Brooks Cole

Avnir D (1989) *The Fractal Approach to Heterogeneous Chemistry: Surfaces, Colloids, Polymers*. Wiley, Chichester.

Banfield JF, Nealson KH (eds) (1997) *Geomicrobiology: Interactions Between Microbes and Minerals*. *Rev Mineral Geochem Vol 35*, Mineralogical Society of America, Washington, DC

Banfield JF, Navrotsky A (eds) (2001) *Nanoparticles in the Environment*. *Rev Mineral Geochem Vol 44*, Mineralogical Society of America, Washington, DC

Banfield JF, Welch SA, Zhang H, Ebert TT, Penn RL (2000). Aggregation-based crystal growth and microstructure development in natural iron oxyhydroxide biomineralization products. *Science* 289:751– 754

Barbara PF, Meyer, TJ, Ratner, MA (1996) Contemporary Issues in Electron Transfer Research. *J Phys Chem* 100:13148-13168

Bard AJ, Fox MA (1995) Artificial photosynthesis – solar splitting of water to hydrogen and oxygen. *Acc Chem Res* 28:141-145

- Bargar JR, Tebo BM, Villinski JE (2000) In situ characterization of Mn(II) oxidation by spores of the marine *Bacillus* sp. strain SG-1. *Geochem Cosmochim Acta* 64:2775-2778.
- Bargar JR, Tebo BM, Bergmann, U, Webb SM, Glatzel P, Chiu VQ, Villalobos M. (2005) Biotic and abiotic products of Mn(II) oxidation by spores of the marine *Bacillus* sp. strain SG-1. *Am Mineral* 90:143-154
- Bazylnski DA, Frankel RB (2004) Magnetosome formation in prokaryotes. *Nature Reviews Microbiology* 2:217-230
- Bebie J, Schoonen MAA, Fuhrmann M, Strongin DR (1998) Surface charge development on transition metal sulfides: An electrokinetic study *Geochim Cosmochim Acta* 62:633-642
- Bekyarova E, Fornasiero P, Kaspar J, Graziani M (1998) CO oxidation on Pd/CeO₂-ZrO₂ catalysts. *Catalysis Today* 45:179-183
- Belin T, Millot N, Villieras F, Bertrand O, Bellat JP (2004) Structural variations as a function of surface adsorption in nanostructured particles. *J Phys Chem B* 108:5333-5340
- Benner, S. G., Hansel, C. M., Wielinga, B. W., Barber, T. M., & Fendorf, S. (2002) Reductive dissolution and biomineralization of iron hydroxide under dynamic flow conditions. *Environ Sci Technol* 36:1705–1711.
- Benning L, Wilkin RT, Barnes HL. (2000) Reaction pathways in the Fe-S system below 100°C. *Chemical Geology* 167:25–51
- Berhault G, Lacroix M, Breyse M, Maugé F, Lavalley JC, Nie H, Qu L (1998) Characterization of acidic sites of silica-supported transition metal sulfides by pyridine and 2,6 dimethylpyridine adsorption: Relation to activity in CH₃SH condensation. *J Catalysis* 178:555–565
- Beveridge TJ (1981) Ultrastructure, chemistry and function of the bacterial cell wall. *Int Rev Cytol* 72:229-317
- Billinge SJL, Thorpe MF, eds. (1998) *Local Structure from Diffraction*. Plenum Press, New York
- Bolton JL, Trush MA, Penning TM, Dryhurst G, Monks TJ (2000) Role of quinones in toxicology. *Chemical Research in Toxicology* 13:135-160
- Bourg ACM, Bertin C (1996) Diurnal variations in the water chemistry of a river contaminated by heavy metals: Natural biological cycling and anthropic influence. *Water Air Soil Pollution* 86:101-116

- Boström M, Williams DRM, Ninham BW (2001) Specific ion effects: Why DLVO theory fails for biology and colloid systems. *Phys Rev Lett* 87: 168103
- Bratina BJ, Stevenson BS, Green WJ, Schmidt TM (1998) Manganese reduction by microbes from oxic regions of the Lake Vanda (Antarctica) water column. *Appl Environ Microbiol* 64:3791-3797
- Brown GE, Jr, Foster AL, Ostergren JD (1999) Mineral surfaces and bioavailability of heavy metals: A molecular scale perspective. *Proc Natl Acad Sci* 96:3388-3395
- Brus LEA (1983) Simple model for the ionization potential, electron affinity, and aqueous redox potentials of small semiconductor crystallites. *J Chem Phys* 79:5566-5571
- Brus LEA (1984) Electron-electron and electron-hole interactions in small semiconductor crystallites: The size dependence of the lowest excited electronic state. *J Chem Phys* 80:4403-4409
- Brus LEA (1996) Model for carrier dynamics and photoluminescence quenching in wet and dry porous silicon thin films. *Phys Rev B* 53:4649-4656
- Bryan JD, Heald SM, Chambers SA, Gamelin DR (2004) Strong room-temperature ferromagnetism in Co²⁺-doped TiO₂ made from colloidal nanocrystals. *J Am Chem Soc* 126:11540-11647
- Büker K, Fiechter S, Eyert V, Tributsch H (1999) Photochemistry of highly Zn-doped pyrite as compared with isostructural FeS₂. *J. Electrochem Soc* 146:261-265
- Burns RG, Burns RM (1979) Marine minerals. *Rev Mineral* 6:1-46
- Car R, Parrinello M (1985) Unified approach for molecular dynamics and density functional theory. *Phys Rev Lett* 55:2471-2473
- Cartoixa X, Wang LW (2005) Microscopic dielectric response functions in semiconductor quantum dots. *Phys Rev Lett* 94:236804
- Casey, WH, Swaddle, TW (2003) Why small? The use of small inorganic clusters to understand mineral surface and dissolution reactions in geochemistry. *Rev Geophys* 41:1-20
- Cheah SF, Kraemer SM, Cervini-Silva J, Sposito G (2003) Steady state dissolution kinetics of goethite in the presence of Desferrioxamine-B and oxalate ligands: Implications for the microbial acquisition of iron. *Chemical Geology* 198:63–75
- Chen W, Wang ZG, Lin ZJ, Lin LY (1997) Absorption and luminescence of the surface states in ZnS nanoparticles. *J Appl Phys* 82:3111-3115

- Cheng L, Fenter P, Nagy KL, Schlegel ML, Sturchio MC. (2001) Molecular-scale density oscillations in water adjacent to a mica surface. *Phys Rev Lett* 87:156103
- Cornell RM, Schwertmann U. (1979) Influence of organic anions on the crystallization of ferrihydrite. *Clays Clay Miner* 27:402-410
- Cornell RM, Schwertmann U (2003) *The Iron Oxides: Structure, Properties, Reactions, Occurrences and Uses*. Wiley-VCH, Weinheim
- Davis KJ, Dove PM, De Yoreo JJ (2000) The role of Mg^{2+} as an impurity in calcite growth. *Science* 290:1134-1137
- Delerue C, Allan G, Lannoo M (2001) Electron-phonon coupling and optical transitions for indirect-gap semiconductor nanocrystals. *Phys Rev B* 64:193402
- De Yoreo JJ, Vekilov PG (2003) Principles of nucleation and growth. *Rev Mineral Geochem* 54:57-93
- Dickinson E (1989) Structure of simulated colloidal deposits. *Colloids Surfaces* 39:143-159
- Dos Santos Afonso M, Stumm W (1992) Reductive dissolution of iron(III) (hydr)oxides by hydrogen sulfide. *Langmuir* 8:1671-1675
- Douglas S, Beveridge TJ (1998) Mineral formation by bacteria in natural microbial communities. *FEMS Microbiology Ecology* 26:79-88
- Drits VA, Tchoubar C (1990) X-ray diffraction by disordered lamellar structures: Theory and applications to microdivided silicates and carbons, 371 p. Springer Verlag, Berlin.
- Duonghong D, Ramsden J, Grätzel M (1982) Dynamics of interfacial electron-transfer processes in colloidal semiconductor systems. *J Am Chem Soc* 104:2977-2985
- Dwarakanath S, Bruno JG, Shastry A, Phillips T, John A, Kumar A, Stephenson LD (2004) Quantum dot-antibody and aptamer conjugates shift fluorescence upon binding bacteria. *Biochem Biophys Res Commun* 325:739–743
- Edelbro R, Sandström A, Paul J (2003) Full potential calculations on the electronic bandstructure of sphalerite, pyrite and chalcopyrite. *Appl Surf Sci* 206:300-313
- Edwards KJ, Bond PJ, Gihring TM, Banfield JF. (2000) An archaeal iron-oxidizing extreme acidophile important in acid mine drainage. *Science* 287:1796-1799
- Efros AL, Rosen M (2000) The electronic structure of semiconductor nanocrystals. *Annu Rev Mater Sci* 30:475–521

- Ehrlich HL (2002) Geomicrobiology. Marcel Dekker, New York
- Elimelech M, Gregory J, Jia X, Williams R (1995) *Particle Deposition and Aggregation: Measurement, Modelling and Simulation*. Butterworth Heinemann, Oxford
- Elsner M, Schwarzenbach RP, Haderlein SB (2004) Reactivity of Fe(II)-bearing minerals to reductive transformation of organic contaminants. *Environ Sci Technol* 38:799-807
- Ennaoui A, Tributsch H (1986) Light-induced electron transfer and photoelectrocatalysis of chlorine evolution at FeS₂ electrodes. *J Electroanal Chem* 205:185-195
- Eng PJ, Trainor TP, Brown GE, Waychunas GA, Newville M, Sutton SR, Rivers ML (2000) Structure of the hydrated alpha-Al₂O₃ (0001) surface. *Science* 288:1029-1033
- Oberdorster G, Oberdorster E, Oberdorster J (2005) Nanotoxicology: An emerging discipline evolving from studies of ultrafine particles. *Environ Health Perspectives* 113:823-839
- Erwin SC, Zu L, Haftel, MI, Efros, AL, Kennedy, TA, Norris, DJ (2005) Doping semiconductor nanocrystals. *Nature* 436:91-95
- Ferreya JM, Proetto CR (1999) Quantum size effects on excitonic Coulomb and exchange energies in finite-barrier semiconductor quantum dots. *Phys Rev B* 60:10672-10675
- Ferris FG (2005) Biogeochemical properties of bacteriogenic iron oxides. *Geomicrobiology J* 22:79-85
- Fistul VI (2004) *Impurities in Semiconductors : Solubility, Migration, and Interactions*. CRC Press, Boca Raton, Florida
- Fortin D, Ferris FF, Beveridge TJ (1997) Surface-mediated mineral development by bacteria. *Rev Mineral Geochem* 35: 161–180
- Fowler TA, Holmes PR, Crundwell FK (1999) Mechanism of pyrite dissolution in the presence of *Thiobacillus ferrooxidans*. *Appl Environ Microbiol* 65:2987-2993
- Franceschetti A, Zunger A (1997) Direct pseudopotential calculations of exciton Coulomb and exchange energies in semiconductor quantum dots. *Phys Rev Lett* 78:915-917
- Franceschetti A, Williamson A, Zunger A (2000) Addition spectra of quantum dots: The role of dielectric mismatch. *J Phys Chem B* 104:3398-3401
- Frankel RB, Bazylinski DA Biologically induced mineralization by bacteria. (2003) *Rev Mineral Geochem* 54:95-114

- Fredrickson JK, Zachara JM, Kennedy DW, Duff MC, Gorby YA (2000) Reduction of U(VI) in goethite (α -FeOOH) suspensions by a dissimilatory metal-reducing bacterium. *Geochim Cosmochim Acta* 64:3085-3098
- Fredrickson JK, Kota S, Kukkadapu RK, Liu C, Zachara JM (2003) Influence of electron donor/acceptor concentrations on hydrous ferric oxide (HFO) bioreduction. *Biodegradation* 14:91–103
- Fukushi K, Sato T (2005) Using a surface complexation model to predict the nature and stability of nanoparticles. *Environ Sci Technol* 39:1250-1256
- Fujimori A, Saeki M, Kimizuka N, Taniguchi M, Suga S (1986) Photoemission satellites and electronic structure of α -Fe₂O₃. *Phys Rev B* 34:7318-7327
- Fujita E, DuBois DL (2003) Carbon dioxide fixation. In: Archer MD, Nozik AJ (eds) *Photoconversion of Solar Energy Photochemical and Photoelectrochemical Approaches to Solar Energy Conversion*. Imperial College Press, London
- Fujiwara H, Kanemoto M, Ankyu H, Murakoshi K, Wada Y, Yanagida S (1997) Visible-light induced photofixation of carbon dioxide into aromatic ketones and benzyl halides catalyzed by CdS nanocrystals. *J Chem Soc Perkin Trans 2*:317-321
- Fujiwara H, Hosokawa H, Murakoshi K, Wada Y, Yanagida S (1998) Surface Characteristics of ZnS nanocrystallites relating to their photocatalysis for CO₂ reduction. *Langmuir* 14:5154-5159
- Galli G (2005) Doping the undopable. *Nature* 436:32-33
- Galli G, Parrinello M (1992) Large scale electronic structure calculations. *Phys Rev Lett* 69:3547-3550
- Gaponenko SV (1998) *Optical Properties of Semiconductor Nanocrystals*. Cambridge University Press, Cambridge.
- Garrett BC et al. (2005) Role of water in electron-initiated processes and radical chemistry: Issues and scientific advances. *Chem Rev* 105:355–389
- Gerischer S (1970) **TITLE** in *Physical Chemistry*, Eyring M et al., eds. Academic Press, New York.
- Gerischer S (1980) Photodecomposition of semiconductors: Thermodynamics, kinetics and application to solar cells. *Faraday Disc Chem Soc* 70:137-151

Gerischer S (1993) Photoelectrochemical catalysts of the oxidation of organic molecules by oxygen on small semiconductor particles with TiO₂ as an example. *Electrochim Acta* 38:3-9

Gilbert B, Huang F, Zhang HZ, Waychunas GA, Banfield JF (2004) Nanoparticles: Strained and stiff. *Science* 305:651-654

Gilbert B, Frazer BH, Belz A, Conrad PG, Neelson KH, Haskel D, Lang JH, Srajer G, De Stasio G (2003) Multiple scattering calculations of bonding and x-ray absorption spectroscopy of manganese oxides. *J Phys Chem A* 107:2839-2847

Gratzel M, Frank A (1982) Interfacial electron-transfer reactions in colloidal semiconductor dispersions. Kinetic analysis. *J Phys Chem* 86:2964-2967

Green M, O'Brien P (1999) Recent advances in the preparation of semiconductors as isolated nanometric particles: new routes to quantum dots. *Chem Commun* 22:2235-2241

Guo J (2004) Synchrotron radiation, soft-X-ray spectroscopy and nanomaterials. *Int. J. of Nanotechnology* 1:193-225

Gunnars A, Blomqvist S, Johansson P, Andersson C (2002) Formation of Fe(III) oxyhydroxide colloids in freshwater and brackish seawater, with incorporation of phosphate and calcium. *Geochim Cosmochim Acta* 66:745-758

Haack EA, Warren LA (2003) Biofilm hydrous manganese hydroxides and metal dynamics in acid rock drainage. *Environ Sci Technol* 37:4138-4147

Hall EJ (2000) *Radiobiology for the Radiologist*. Lippincott Williams & Wilkins

Hansel CM, Benner SG, Neiss J, Dohnalkova A, Kukkadapu RK, Fendorf S (2003) Secondary mineralization pathways induced by dissimilatory iron reduction of ferrihydrite under advective flow *Geochim Cosmochim Acta* 67:2977-2992

Hansel CM, Benner SG, Nico P, Fendorf S (2004) Structural constraints of ferric (hydr)oxides on dissimilatory iron reduction and the fate of Fe(II). *Geochim Cosmochim Acta* 68:3217-3229

Haram SK, Quinn BN, Bard AJ (2001) Electrochemistry of CdS nanoparticles: A correlation between optical and electrochemical band gaps. *J Am Chem Soc* 123:8860-8861

Henderson MA (2002) The interaction of water with solid surfaces: Fundamental aspects revisited. *Surface Science Reports* 46:5-308

Hering JG, Stumm W (1990) Oxidative and reductive dissolution of minerals. *Rev Mineral* 23:427-464

- Hill NA, Whaley KB (1995) Size dependence of excitons in silicon nanocrystals. *Phys Rev Lett* 75:1130-1133
- Hochella MF, Jr., White AF (eds) (1990) Mineral-water interface geochemistry. *Reviews in Mineralogy Vol 23*, Mineral Society of America, Washington DC
- Hochella MF, Jr., Moore JN, Putnis C, Putnis A, Kasama T, and Eberl DD (2005a) Direct observation of toxic metal-mineral association from a massive acid mine drainage system: Implications for metal transport and bioavailability. *Geochem Cosmochim Acta*, 69:1651-1663
- Hochella MF, Jr., Kasama T, Putnis A, Putnis C, Moore JN (2005b) Environmentally important, poorly crystalline Fe/Mn hydrous oxides: Ferrihydrite and a vernadite-like mineral from a massive acid mine drainage system. *Am Mineral* 90:718-724.
- Huber R, Spörlein S, Moser JE, Grätzel M (2000) The role of surface states in the ultrafast photoinduced electron transfer from sensitizing dye molecules to semiconductor colloids. *J Phys Chem B* 104:8995-9003
- Inoue H, Moriwaki H, Maeka K, Yoneyama H (1995) Photoreduction of carbon-dioxide using chalcogenide semiconductor nanocrystals. *J Photochem Photobiol A* 86:191-196
- Ireta J, Galván M, Cho K, Joannopoulos JD (1998) Local reactivity of charybdotoxin, a K^+ channel blocker. *J Am Chem Soc* 120:9771-9778
- Isaure MP, Manceau A, Tamura NO, Marcus MA (2005) Zinc mobility and speciation in soil covered by contaminated dredged sediment using micrometer-scale and bulk-averaging X-ray fluorescence, absorption and diffraction techniques. *Geochim Cosmochim Acta* 69:1173-1198
- Israelachvili J. (1992) *Intermolecular and Surface Forces*. Academic Press, San Diego.
- Iwamoto M, Abe T, Tachibana Y (2000) Control of bandgap of iron oxide through its encapsulation into SiO_2 -based mesoporous materials.
- Hoffmann MR, Martin ST, Choi W, Bahneman DW (1995) Environmental applications of semiconductor photocatalysis. *Chem Rev* 95: 69-96
- Jones F, Cölfen H, Antonietti M (2000) Iron oxyhydroxide colloids stabilized with polysaccharides. *Colloid Polym Sci* 278:491-501
- Kagan CR, Murray CB, Bawendi MG (1996) Long-range resonance transfer of electronic excitations in close-packed CdSe quantum-dot solids. *Phys Rev B* 54:8633-8643

- Kennedy CB, Scott SD, Ferris FG (2004) Hydrothermal phase stabilization of 2-line ferrihydrite by bacteria. *Chemical Geology* 212:269-277
- Kennedy CB, Scott SD, Ferris FG (2003a) Characterization of bacteriogenic iron oxide: Deposits from Axial Volcano, Juan de Fuca Ridge, Northeast Pacific Ocean. *Geomicrobiol J* 20:199-214
- Kennedy CB, Scott SD, Ferris FG (2003b) Ultrastructure and potential sub-seafloor evidence of bacteriogenic iron oxides from Axial Volcano, Juan de Fuca Ridge, north-east Pacific Ocean. *FEMS Microbiol Ecol* 43:247-254
- Kerisit S, Cooke DJ, Spagnoli D, Parker SC (2005) Molecular dynamics simulations of the interactions between water and inorganic solids. *J Mater Chem* 15:1454-1462
- Kimball BA, Callender E, Axtmann EV (1995) Effects of colloids on metal transport in a river receiving acid-mine drainage, Upper Arkansas River, Colorado, USA. *Appl Geochem* 10:285-306
- Kloepfer JA, Mielke RE, Nadeau JL (2005) Uptake of CdSe and CdSe/ZnS quantum dots into bacteria via purine-dependent mechanisms. *Appl Environ Microbiol* 71:2548-2557
- Konhauser KO (1998) Diversity of bacterial iron mineralization. *Earth Science Reviews* 43:91-121
- Konovalova TA, Konovalov VV, Kispert LD (1999) Surface modification of TiO₂ nanoparticles with carotenoids. *EPR Study. J Phys Chem B* 103:4672-4699
- Konovalova TA, Lawrence J, Kispert LD (2004) Generation of superoxide anion and most likely singlet oxygen in irradiated TiO₂ nanoparticles modified by carotenoids. *J Photochem Photobiol A* 162:1-8
- Kormann C, Bahnemann DW, Hoffmann MR (1989) Environmental photochemistry: Is iron oxide (hematite) an active photocatalyst? A comparative study: α -Fe₂O₃, ZnS, TiO₂. *J Photochem. Photobiol A* 48:161-169
- Kormann C, Bahnemann DW, Hoffmann MR (1991) Photolysis of chloroform and other organic molecules in aqueous TiO₂ suspensions. *Environ Sci Technol* 25:494-500
- Kraemer SM (2004) Iron oxide dissolution and solubility in the presence of siderophores. *Aquatic Sci* 66:3-88.
- Kucur E, Riegler J, Urban GA, Nann T (2003) Determination of quantum confinement in CdSe nanocrystals by cyclic voltammetry. *J Chem Phys* 119: 2333-2337

Labrenz M, Druschel GK, Thomsen-Ebert T, Gilbert B, Welch SA, Kemner KM, Logan GA, Summons RE, De Stasio G, Bond PL, Lai B, Kelly SD, Banfield JF (2000) Sphalerite (ZnS) deposits forming in natural biofilms of sulfate-reducing bacteria. *Science* 290:1744-1747

Landolt-Bernstein (1983) Numerical data and functional relationships in science and technology, New Series Springer, Berlin

Langmuir D (1996) Aqueous Environmental Geochemistry. Prentice Hall

Lawless D, Sepone N, Meisel D (1991) Role of OH[•] radicals and trapped holes in photocatalysis. A pulse radiolysis study. *J. Phys Chem* 95:5166-5170

Leland JK, Bard AJ (1987) Photochemistry of colloidal semiconducting iron oxide polymorphs. *J Phys Chem* 91:5076-5083

Lewis EA, Smith JRL, Walton PH, Archibald SJ, Foxton SP, Giblin GMP (2001) Tuning the metal-based redox potentials of manganese *cis*, *cis*-1,3,5-triaminohexane complexes. *J Chem Soc Dalton Trans* 2001:1159-1161

Lippens PE, Lannoo M (1989) Calculations of band gap for small CdS and ZnS crystallites. *Phys Rev B* 39:10935-10941

Lodziana Z, Topsoe NY, Norskov JK (2004) A negative surface energy for alumina. *Nature Materials* 3:289-293

Lovely DR (1987) Organic matter mineralization with the reduction of ferric iron: A review. *Geomicrobiol J* 5:375-399

Lovley DR, Stolz JF, Nord GL, Phillips EJP (1987) Anaerobic production of magnetite by a dissimilatory iron-reducing microorganism. *Nature* 330:252-254

Lovely DR, Phillips EJP, Gorby YA, Landa ER (1991) Microbial reduction of uranium. *Nature* 350:413-416

Lovely DR (1993) Dissimilatory metal reduction. *Ann Rev Microbiol* 47:263-290

Lovely DR (1997) Microbial Fe(III) reduction in subsurface environments. *FEMS Microbiol Rev* 20:305-313.

Lucas E, Decker S, Khaleel A, Seitz A, Fultz S, Ponce A, Carnes C, Klabunde KJ (2001) Nanocrystalline metal oxides as unique chemical reagents/sorbents. *Chem Eur J* 7:2505-2510

Lüning J, Rockenberger J, Eisbitt S, Rubensson JE, Karl A, Kornowski A, Weller H, Eberhardt W (1999) Soft x-ray spectroscopy of single size CdS nanocrystals: Size confinement and electronic structure. *Solid State Commun* 112:5-9

Lyklema J (2001) *Fundamentals of Interface and Colloid Science Volume II: Solid-Liquid Interfaces*. Academic Press, San Diego.

Madden AS, Hochella MF, Jr (2005) A test of geochemical reactivity as a function of mineral size: Manganese oxidation promoted by hematite nanoparticles. *Geochim Cosmochim Acta* 69:389-398

Manceau A, Drits, VA Silvester E, Bartoli C, Lanson B (1997) Structural mechanism of Co^{2+} oxidation by the phyllo-manganate buserite. *Am Mineral* 82:1150-1175

Manceau A, Tommaseo C, Rihs S, Geoffroy N, Chateigner D, Schlegel M, Tisserand D, Marcus MA, Tamura M, Chen ZS (2005) Natural speciation of Mn, Ni, and Zn at the micrometer scale in a clayey paddy soil using X-ray fluorescence, absorption, and diffraction. *Geochim Cosmochim Acta* (in press).

Mann S (2000) *Biomineralization*. Oxford University Press, Oxford

Marcus MA (1993) Electron transfer reactions in chemistry. Theory and experiment. *Rev Mod Phys* 65:599-610

Mayers IT, Beveridge TJ (1989) The sorption of metals to *Bacillus subtilis* walls from dilute solutions and simulated Hamilton Harbour (Lake Ontario) water. *Can J Microbiol* 35:764-770

McCormick ML, Bouwer EJ, Adriaens (2002) Carbon tetrachloride transformation in a model iron-reducing culture: Relative kinetics of biotic and abiotic reactions. *Environ Sci Technol* 36:403-410

McCormick ML, Adriaens P (2004) Carbon tetrachloride transformation on the surface of nanoscale biogenic magnetite nanoparticles. *Environ Sci Technol* 38:1045-1053

McKenzie KJ, Marken F (2001) Direct electrochemistry of nanoparticulate Fe_2O_3 in aqueous solution and adsorbed onto tin-doped indium oxide. *Pure Appl Chem* 73:1885-1894

Meakin P (1988) Fractal aggregates. *Adv. Colloid Interface Sci.* 28:249-331

Memming R (2001) *Semiconductor Electrochemistry*. Wiley-VCH, Weinheim.

Missana T, Maffiotte C, García-Gutiérrez M (2003) Surface reaction kinetics between nanocrystalline magnetite and uranyl. *J Colloid Interf Sci* 261:154-160

Monticone S, Tufeu R, Kanaev AV, Scolan E, Sanchez C (2000) Quantum size effect on TiO₂ nanoparticles: Does it exist? *Appl Surf Sci* 162-163:565-570

Moreau JW, Webb RI, Banfield JF (2004) Ultrastructure, aggregation state and crystal growth of biogenic nanocrystalline sphalerite and wurtzite. *Am Mineral* 89:950-960.

Morrison SR (1980) *Electrochemistry at Semiconductor and Oxidized Metal Interfaces*. Plenum Press, New York

Moser J, Punchedhewa S, Infelta PP, Gratzel M (1991) Surface complexation of colloidal semiconductors strongly enhances interfacial electron-transfer rates. *Langmuir* 7:3012-3018

Moser CC, Keske JM, Warncke K, Farid RS, Dutton PL (1992) Nature of biological electron transfer. *Nature* 355:796-802

Müller BR, Majoni S, Memming R, Meissner D (1997) Particle size and surface chemistry in photoelectrochemical reactions at semiconductor particles. *J Phys Chem B* 101:2501-2507

Mulvaney P, Cooper R, Grieser F, Meisel D (1988) Charge trapping in the reductive dissolution of colloidal suspensions of iron(III) oxides. *Langmuir* 4: 1206-1211

Murray JW, Dillard JG (1979) The oxidation of cobalt(II) adsorbed on manganese dioxide. *Geochim Cosmochim Acta* 43:781-787

Murray CB, Kagan CR, Bawendi MG (2000) Synthesis and characterization of monodisperse nanocrystals and close-packed nanocrystal assemblies. *Annu Rev Mater Sci* 30:545-610

Mylon SE, Chem KL, Elimelech M (2004) Influence of natural organic matter and ionic composition on the kinetics and structure of hematite colloid aggregation: Implications to iron depletion in estuaries. *Langmuir* 20:9000-9006

Nanda KK, Kruis FE, Fissan H, Behera SN (2004) Effective mass approximation for two extreme semiconductors: Band gap of PbS and CuBr nanoparticles. *J Appl Phys* 95:5035-5041

Navrotsky A (2004) Energetic clues to pathways to biomineralization: Precursors, clusters and nanoparticles. *Proc Natl Sci Acad* 101:12096-12101

Nedeljkovic JM, Nenadovic MT, Micic OI, Nozik AJ (1986) Enhanced photoredox chemistry in quantized semiconductor colloids. *J Phys Chem* 90:12-13

Nelson J (1999) Continuous-time random walk model of electron transport in nanocrystalline TiO₂ electrodes. *Phys Rev B* 59:15374-15380

- Newman DK, Kolter R (2000) A role for excreted quinines in extracellular electron transfer. *Nature* 405:94-97
- Nevin KP, Lovley DR (2000) Potential for nonenzymatic reduction of Fe(III) via electron shuttling in subsurface sediments. *Environ Sci Technol* 34:2472-2478
- Noguera C, Pojani A, Casek P, Finocchi F (2002) Electron redistribution in low-dimensional oxide structures. *Surface Science* 507-510:245-255
- Oberdorster G, Oberdorster E, Oberdorster J (2005) Nanotoxicology: An emerging discipline evolving from studies of ultrafine particles. *Environ Health Perspectives* 113:823-839
- O'Connor MV, Sposito G (2004) Investigation of biogenic manganese oxide by density functional theory. *Abstr Papers Am Chem Soc* 228:U548-549 043-ENVR
- O'Loughlin EJ, Kelly SD, Cook RE, Csencsits R, Kemner KM (2003) Reduction of uranium(VI) by mixed iron(II)/iron(III) hydroxide (green rust): Formation of UO₂ nanoparticles. *Environ Sci Technol* 37:721-727.
- Palosz B, Grzanka E, Gierlotka S, Stel'Mahk S, Pielaszek R, Bismayer U, Neuefeind J, Weber HP, Palosz W (2002) Diffraction studies of nanocrystals: Theory and experiment. *Acta Physica Polonica* 102:57-82
- Page CC, Moser CC, Chen X, Dutton L (1999) Natural engineering principles of electron tunnelling in biological oxidation-reduction. *Nature* 402:47-52
- Parak WJ, Boudreau R, Le Gros M, Gerion D, Zanchet D, Micheel CM, Williams SC, Alivisatos AP, Larabell C (2002) Cell motility and metastatic potential studies based on quantum dot imaging of phagokinetic tracks. *Adv Mater* 14:882-885
- Patterson AL (1939) The Scherrer formula for x-ray particle size determination. *Phys Rev* 56:978-982
- Park H, Choi W (2005) Photocatalytic conversion of benzene to phenol using modified TiO₂ and polyoxometalates. *Catalysis Today* 101:291-297
- Parak WJ, Boudreau R, Le Gros M, Gerion D, Zanchet D, Micheel CM, Williams SC, Alivisatos AP, Larabell C (2002) Cell motility and metastatic potential studies based on quantum dot imaging of phagokinetic tracks. *Adv Mater* 14:882-885
- Park JH, Tjeng LH, Allen JW, Metcalf P, Chen CT (1997) Single-particle gap above the Verwey transition in Fe₃O₄. *Phys Rev B* 57:12813-12817

Peak D (2005) In situ ATR-FTIR spectroscopic studies of the kinetics of oxyanion/metal oxide adsorption. *Abstr Papers Am Chem Soc* 228:U900 113-GEOC

Pecher K, Haderlein SB, Schwartzbach RP (2002) Reduction of polyhalogenated methanes by surface-bound Fe(II) in aqueous suspensions of iron oxides. *Environ Sci Technol* 36:1734-1741

Pehkonen SO, Seifert RL, Hoffman MR (1995) Photoreduction of iron oxyhydroxide and the photooxidation of halogenated acetic acids *Environ Sci Technol* 29:1215-1222

Pellegrini G, Mattei G, Mazzoldi P (2005) Finite depth square well model: Applicability and limitations. *J Appl Phys* 97:073706

Penn RL, Banfield JF (1998) Oriented attachment and growth, twinning, polytypism, and formation of metastable phases: Insights from nanocrystalline TiO₂. *Am Mineral* 83:1077-1082

Penn RL, Zhu C, Xu H, Veblen DR. (2001) Iron oxide coatings on sand grains from the Atlantic coastal plain: High-resolution transmission electron microscopy characterization. *Geology* 29:843-846

Phoenix VR, Konhauser KO, Adams DG, Bottrell SH (2001) Role of biomineralization as an ultraviolet shield: Implications for Archean life. *Geology* 29:823-826

Poddar P, Fried T, Markovich G (2002) First-order metal-insulator transition and spin-polarized tunneling in Fe₃O₄ nanocrystals. *Phys Rev B* 65: 172405

Pokrant S and Whaley KB (1999) Tight-binding studies of surface effects on electronic structure of CdSe nanocrystals: The role of organic ligands, surface reconstruction and inorganic capping shells. *European Journal of Physics* 6:255-267

Poulton SW, Krom MD, Raiswell R (2004) A revised scheme for the reactivity of iron (oxyhydr)oxide minerals towards dissolved sulfide. *Geochim Cosmochim Acta* 68:3703-3715

Preisinger M, Krispin M, Rudolf T, Horn S, Strongin DR (2005) Electronic structure of nanoscale iron oxide particles measured by scanning tunneling and photoelectronic spectroscopies. *Phys Rev B* 71:165409

Puzder A, Williamson AJ, Reboredo FA, Galli G (2003) Structural stability and optical properties of nanomaterials with reconstructed surfaces. *Phys Rev Lett* 91:157405

Qadri SB, Skelton EF, Dinsmore AD, Yang J, Gray HF, Ratna BR (1999) Size-induced transition-temperature reduction in nanoparticles of ZnS. *Phys Rev B* 60:9191-9193

Quantin C, Becquer T, Rouiller JH, Berthelin J (2001) Oxide weathering and trace metal release by bacterial reduction in a New Caledonia Ferralsol. *Biogeochemistry* 53:323-340

Rabani E, Hetenyi B, Berne BJ (1999) Electronic properties of CdSe nanocrystals in the absence and presence of a dielectric medium. *J Chem Phys* 110:5355-5368

Rabani E (2001) Structure and electrostatic properties of passivated CdSe nanocrystals. *J Chem Phys* 115:1493-1497

Rajh T, Chen LX, Lukas K, Liu T, Thurnauer MC, Tiede DM (2002) Surface restructuring of nanoparticles: An efficient route for ligand-metal oxide crosstalk. *J Phys Chem B* 106: 10543- 10552

Rajh T, Saponjic Z, Liu JQ, Dimitrijevic NM, Scherer NF, Vega-Arroyo M, Zapol P, Curtiss LA, Thurnauer MC (2004) Charge transfer across the nanocrystalline-DNA interface: Probing DNA recognition. *Nano Lett* 4:1017-1023

Rancourt DG (2001) Magnetism of earth, planetary and environmental nanomaterials. *Rev Mineral Geochem* 44:217–292

Rancourt DG, Thibault PJ, Mavrocordatos D, Lamarche G (2005) Hydrous ferric oxide precipitation in the presence of nonmetabolizing bacteria: Constraints on the mechanism of a biotic effect. *Geochim Cosmochim Acta* 69:553-577

Redl FX, Black CT, Papaefthymiou GC, Sandstrom RL, Yin M, Zeng H, Murray CB, O'Brien SP (2004) Magnetic, electronic, and structural characterization of nonstoichiometric iron oxides at the nanoscale. *J Am Chem Soc* 126:14583-14599

Reguera G, McCarthy KD, Mehta T, Nicoll JS, Tuominen MT, Lovley DR (2005) Extracellular electron transfer via microbial nanowires. *Nature* 435:1098-1101

Roden EE, Zachara JM (1996) Microbial reduction of crystalline iron (III) oxides: Influence of oxide surface area and potential for cell growth. *Environ Sci Technol* 30:1618-1628

Roden EE, Urrutia MM, Mann, CJ (2000) Bacterial reductive dissolution of crystalline Fe(III) oxide in continuous-flow column reactors. *Appl. Environ Microbiol* 66:1062-1065

Rodriguez JA, Chaturvedi S, Kuhn M, Hrbek J (1998) Reaction of H₂S and S₂ with metal/oxide surfaces: Band-gap size and chemical reactivity. *J Phys Chem B* 102:5511-5519

Rosso KM, Smith DMA, Dupuis M (2003) An *ab initio* model of electron transport in hematite (α -Fe₂O₃) basal planes. *J Chem Phys* 118:6455-6466

- Rozan TF, Lassman ME, Ridge DP, Luther GW (2000) Evidence for iron, copper and zinc complexation as multinuclear sulphide clusters in oxic rivers. *Nature* 406:879-882
- Rustad JR, Felmy AR (2005) The influence of edge sites on the development of surface charge on goethite nanoparticles: A molecular dynamics investigation. *Geochim Cosmochim Acta* 69:1405-1411
- Scholz F, Meyer B (1998) Voltammetry of solid microparticles immobilized on electrode surfaces. *Electroanal Chem* 20:1-86
- Schooss D, Mews A, Eychmüller A, Welller H (1994) Quantum-dot quantum well CdS/HgS/CdS: Theory and experiment. *Phys Rev B* 49:17072-17078
- Schüring J, Schulz HD, Fischer WR, Böttcher J, Duijnsveld WHM (2000) *Redox: Fundamental Processes and Applications*. Springer-Verlag, Berlin
- Schwertmann U, Gasser U, Sticher H (1989) Chromium-for-iron substitution in synthetic goethites. *Geochim Cosmochim Acta* 53:1293-1297
- Schwertmann U, Pfab G (1994) Structural vanadium in synthetic goethite. *Geochim Cosmochim Acta* 58:4349-4352
- Schwertmann U, Friedl J, Stanjek, H (1999) From Fe(III) ions to ferrihydrite and then to hematite. *J Colloid Interf Sci* 209:215-223
- Scott SD, Barnes HL (1972) Sphalerite-wurtzite equilibria and stoichiometry. *Geochim Cosmochim Acta* 36:1276-1295
- Scott DT, McKnight DM, Voelker Bm, Hrcir DC (2002) Redox processes controlling manganese fate and transport in a mountain stream. *Environ Sci Technol* 36:453-459
- Serpone N, Lawless D, Khairutdinovt R (1995) Size Effects on the photophysical properties of colloidal anatase TiO₂ particles: Size quantization or direct transitions in this indirect semiconductor? *J Phys Chem* 99:16646-16654
- Shen H, Tan J, Saltzmann WM (2004) Surface-mediated gene transfer from nanocomposites of controlled texture. *Nature Materials* 3:569-574
- Sherman DM (1984) Electronic structure of manganese oxide minerals. *Am Mineral* 69:788-799
- Sherman DM (1985) Electronic structures of Fe³⁺ coordination sites in iron oxides: applications to spectra, bonding and magnetism. *Phys Chem Mineral* 12:161-175.

Sherman DM (2005) Electronic structures of iron (III) and manganese (IV) (hydr)oxide minerals: Thermodynamics of photochemical reductive dissolution in aquatic sediments. *Geochim Cosmochim Acta* 69:3249-3255

Sparks NHC, Mann S, Bazylinski DA, Lovely DR, Jannasch HW, Franekl RB (1990) Structure and morphology of magnetite anaerobically-produced by a marine magnetotactic bacterium and a dissimilatory iron-reducing bacterium. *Earth Planet Sci Lett* 98:14-22

Stack AG, Erni R, Browning ND, Casey WH (2004) Pyromorphite growth on lead-sulfide surfaces. *Environ Sci Technol* 38:5529-5534

Stone AT, Morgan JJ (1984) Reduction and dissolution of manganese(III) and manganese(IV) oxides by organics. 2. Survey of the reactivity of organics. *Environ Sci Technol* 18:617-624

Stumm W, Morgan JJ (1996) *Aquatic chemistry: Chemical Equilibria and Rates in Natural Waters*. p. 400-414. Wiley, New York

Sunda WG, Huntsman SA, Harvey GR (1983) Photoreduction of manganese oxides in seawater and its geochemical and biological implications. *Nature* 301:234-236

Suzuki Y, Kelly SD, Kemner KM, Banfield JF (2002) Nanometre-size products of uranium bioreduction. *Nature* 419:134-134.

Tang J, Myers M, Bosnik KA, Brus LE (2003) Magnetite Fe₃O₄ nanocrystals: Spectroscopic observation of aqueous oxidation kinetics. *J Phys Chem B* 107:7501-7506

Tartaj P, del Puerto Morales M, Veintemillas-Verdaguer S, González-Carreño T, Serna CJ (2003) The preparation of magnetic nanoparticles for applications in biomedicine. *J Phys D: Appl Phys* 36:R182-R197

Tebo BM, Bargar JR, Clement BG, Dick GJ, Murray KJ, Parker D, Verity R, Webb SM (2004) Biogenic manganese oxides: Properties and mechanisms of formation. *Annu Rev Earth Planet Sci* 32:287-328

Tebo BM, Ghiorse WC, van Waasbergen LG, Siering PL, Caspi R (1997) Bacterially-mediated mineral formation: insights into manganese(II) oxidation from molecular genetic and biochemical studies. *Rev Mineral Geochem* 35:225-266

Templeton AS, Spormann AM, Brown GE (2003) Speciation of Pb(II) sorbed by *Burkholderia cepacia*/goethite composites. *Environ Sci Technol* 37:2166-2172

Thomas TN, Land TA, Johnson M, Casey WH (2004) Molecular properties of adsorbates that affect the growth kinetics of archerite (KDP). *J Colloid Interf Sci* 280:18-26

Tiller CL, O'Melia CR (1993) Natural organic matter and colloidal stability: Models and measurements. *Colloids Surfaces A* 73:89-102

Todo S, Takeshita N, Kanehara T, Mori T, Mri N (2001) Metallization of magnetite (Fe_3O_4) under high pressure. *J Appl Phys* 89:7347-7349

Tolbert SH, Herhold AB, Johnson CS, Alivisatos AP (1994) Comparison of quantum confinement effects on the electronic absorption spectra of direct and indirect gap semiconductor nanocrystals. *Phys Rev Lett* 73:3266-3269

Torres-Martínez CL, Kho R, Mian OI, Mehra RK (2001) Efficient photocatalytic degradation of environmental pollutants with mass-produced ZnS nanocrystals. *J Coll Interf Sci* 240:525-532.

Tran Thoai DB, Hu YZ, Koch SW (1990) Influence of the confinement potential on the electron-hole-pair states in semiconductor microcrystallites. *Phys Rev B* 42:11261-11266.

Trindade T, O'Brien P, Pickett NL (2001) Nanocrystalline semiconductors: Synthesis, properties, and perspectives. *Chem Mater* 13:3847-3858

Tronc E, Belleville P, Jolivet JP, Livage J (1992) Transformation of ferric hydroxide into spinel by Fe(II) adsorption. *Langmuir* 8:313-319

Tronc E, Jolivet JP, Lefevre J, Massart R (1984) Iron adsorption and electron transfer in spinel-like iron oxide colloids. *J Chem Soc* 80:2619-2629

Urrutia MM, Roden, EE, Zachara, JM (1999) Influence of aqueous and solid-phase Fe(II) complexants on microbial reduction of crystalline iron(III) oxides. *Environ Sci Technol* 33:4022-4028

van der Zee C, Roberts DR, Rancourt DG, Slomp CP (2003) Nanogoethite is the dominant reactive oxyhydroxide phase in lake and marine sediments. *Geology* 31:993-996

Vaughan DJ, Craig JR (1978) *Mineral Chemistry of Metal Sulfides*. Cambridge University Press, Cambridge, MA

Vayssières L, Chaneac C, Tronc E, Jolivet JP (1998) Size tailoring of magnetite particles formed by aqueous precipitation: An example of thermodynamic stability of nanometric oxide particles. *J Colloid Interf Sci* 205:205-212

Verwey, E. J. W., & Overbeek, J. Th. G. *Theory of the Stability of Lyophobic Colloids*. Elsevier, Amsterdam, 1948.

- Villalobos M, Toner B, Bargar JR, Sposito G (2003) Characterization of the manganese oxide produced by *Pseudomonas putida* strain MnB1. *Geochim Cosmochim Acta* 67:2649-2662
- Voelker BM, Morel FMM, Sulzberger B (1997) Iron redox cycling in surface waters: Effects of humic substances and light. *Environ Sci Technol* 31:1004-1011
- Vyalikh DV, Dänzenbacher S, Mertig M, Kirchner A, Pompe W, Dedkov, YS, Molodtsov SL (2004) Electronic structure of regular bacterial surface layers. *Phys Rev Lett* 93:238103
- Waite TD (1990) Photo-redox processes at the mineral-water interface. *Rev Mineral* 23:559-603
- Wang CC, Zhang Z, Ying JY (1997) Photocatalytic decomposition of halogenated organics over nanocrystalline titania. *Nanostruct Mater* 9:583-586
- Wang CS, Klein (1981) First-principles electronic structure of Si, Ge, GaP, GaAs, ZnS, and ZnSe. I. Self-consistent energy bands, charge densities, and effective masses. *Phys Rev B* 24:3393-3416
- Wang CY, Böttcher C, Bahnemann DW, Dohrmann JK (2003) A comparative study of nanometer sized Fe(III)-doped TiO₂ photocatalysts: synthesis, characterization and activity. *J Mater Chem* 13:2322-2329
- Wang LG, Pennycock SJ, Pantelides ST (2002) The role of the nanoscale in surface reactions: CO₂ on CdSe. *Phys Rev Lett* 89:075506
- Wang LW, Zunger A (1996) Pseudopotential calculations of nanoscale CdSe quantum dots. *Phys Rev B* 53:9579-9581.
- Warren LA, Ferris FG (1998) Continuum between sorption and precipitation of Fe(III) on microbial surfaces. *Environ Sci Technol* 32:2331-2337
- Warren LA, Haack EA (2001) Biogeochemical controls on metal behaviour in freshwater environments. *Earth-Science Reviews* 54:261-320
- Watson JHP, Cressey BA, Roberts AP, Ellwood DC, Charnock JM, Soper AK (2000) Structural and magnetic studies on heavy-metal-adsorbing iron sulphide nanoparticles produced by sulphate-reducing bacteria. *J Magnetism Magnetic Materials* 214:13-30
- Waychunas GA, Kim CS, Banfield JF (2005) Nanoparticulate iron oxide minerals in soil and sediments: Unique properties and contaminant scavenging mechanism. *J. Nanoparticle Res* in press.

Webb SM, Tebo BM, Bargar JR (2005) Structural influences of sodium and calcium ions on the biogenic manganese oxides produced by the marine *Bacillus sp.*, strain SG-1. *Geomicrobiol J* 22: 181-193

Wielinga B, Mizuba, MM, Hansel CM, Fendorf S (2001) Iron promoted reduction of chromate by dissimilatory iron-reducing bacteria. *Environ Sci Technol* 35:522-527

Williams AGB, Scherer MM (2004) Spectroscopic evidence for Fe(II)-Fe(III) electron transfer at the iron oxide – water interface. *Environ Sci Technol* 38:4782-4790

Williams KH, Ntarlagiannis D, Slater LD, Dohnalkova A, Hubbard SS, Banfield JF (2005) Geophysical imaging of stimulated microbial biomineralization, *Environ Sci Technol* in press.

Wolthers M, van der Gaast SJ, Rickard D. (2003) The structure of disordered mackinawite *Am. Mineral* 88:2007–2015

Xu Y, Schoonen MAA (1995) The stability of thiosulfate in the presence of pyrite in low-temperature aqueous solutions. *Geochim Cosmochim Acta* 59:4605-4622

Xu Y, Schoonen MAA (2000) Absolute energy positions of conduction and valence bands of selected semiconducting minerals. *Am Mineral* 85:543-556

Yariv S, Cross H (1979) *Geochemistry of Colloid Systems*. Springer-Verlag, Berlin

Yu I, Isobe T, Senna M (1996) Optical properties and characteristics of ZnS nanoparticles with homogeneous Mn distribution. *J Phys Chem Solids* 57:373-379

Zhang H, Penn RL, Hamers, RJ, Banfield JF (1999) Enhanced adsorption of molecules on the surface of nanocrystalline particles. *J Phys Chem B* 103:4656-4662

Zhang H, Gilbert B, Huang F, Banfield JF (2003) Water-driven structure transformation in nanoparticles at room temperature. *Nature* 424:1025-1029

Zhang H, Huang F, Gilbert B, Banfield, JF (2003) Molecular dynamics simulations, thermodynamic analysis, and experimental study of phase stability of zinc sulfide nanoparticles. *J Phys Chem B* 107:13051-13060

Zhang JZ (2000) Interfacial charge carrier dynamics of colloidal semiconductor nanoparticles. *J Phys Chem B* 104:7239-7253

Zhang Z, Wang CC, Zakaria R, Ying JY (1998) Role of particle size in nanocrystalline TiO₂-based photocatalysts. *J Phys Chem B* 102:10871-10878